ROTATIONAL BANDS ON FEW-PARTICLE EXCITATIONS OF VERY HIGH SPIN

C.G. ANDERSSON, J. KRUMLINDE, G. LEANDER AND Z. SZYMANSKI

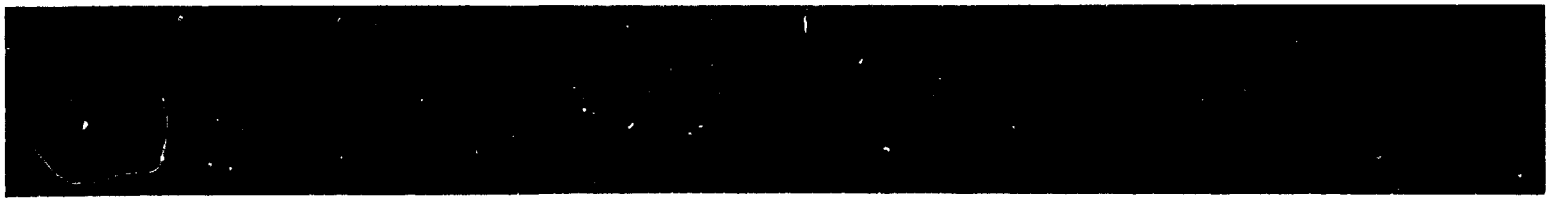

LUND INSTITUTE OF TECHNOLOGY

Department of Mathematical Physics

ROTATIONAL BANDS ON FEW-PARTICLE EXCITATIONS OF VERY HIGH SPIN

C.G. Andersson, J. Krumlinde*, G. Leander and Z. Szymanski**

Department of Mathematical Physics
Lund Institute of Tehcnology
Lund, Sweden

Abstract: An RPA formalism is developed to investigate the existence and properties of slow collective rotation around a non-symmetry axis, when there already exists a large angular momentum K along the symmetry axis built up by aligned single-particle spins. It is found necessary to distinguish between the collectivity and the repeatability of the rotational excitations. First the formalism is applied to bands on high-K isomers in the well-deformed nucleus ^{176}Hf, where the rotational-model picture is reproduced for intermediate K-values in agreement with experiment. At high K there is a suppression of the collectivity corresponding to the diminishing vector-coupling coefficient of the rotational model, but the repeatability actually improves. The moment of inertia is predicted to remain substantially smaller than the rigid-body value so the bands slope up steeply from the yrast line at spins where pairing effects are gone. A second application is to the initially spherical nucleus ^{212}Rn, which is believed to acquire an oblate deformation that increases steadily with K due to the oblate shape of the aligned orbitals. In this case the repeatable excitations come higher above the yrast line than in ^{176}Hf, even at comparable deformations. Some collective states may occur very close to yrast, but these are more like dressed singleparticle excitations. The main differences between the two nuclei studied is interpreted as a general consequence of their different shell structure.

* Address: Department of Physics, University of Lund, Lund, Sweden.

**Visitor supported by NORDITA. Address: Institute of Nuclear Research, Hoza 69, Warsaw, Poland.

1. INTRODUCTION

The spin of a nuclear state can in some cases be simply understood in terms of the shell model as the combined intrinsic spins of one or a few unpaired nucleons, while in other cases collective rotation around a non-symmetry axis would seem to be a more appropriate idealisation. These two limits and the intermediate situations are in themselves interesting to study, but experimental developments over the past decade have also shown that the two modes can coexist and interact in a variety of ways, which are only beginning to be charted and understood. For example, many phenomena observed in collective rotors show how individual quasi-particles may decouple from the ground-state fields in order to align their spins with the angular momentum of the rotor in the yrast states.

In the following we will be concerned with a very different combination of the two modes, where a large angular momentum I=K is generated by the alignment of single-particle spins along a nuclear symmetry axis [1,2], whereupon a relatively small collective rotation giving rise to states I=K+1, K+2, ... may take place around a perpendicular non-symmetry axis. A priori it may be expected that a large K-value will influence the properties and ultimately the existence of such collective bands, for example through changes of the surface and pairing deformations and because of the limited angular momentum available among the valence nucleons. This would reflect structure specific to the nucleus, in contrast for example to an ideal Fermi gas enclosed in a box with a deformation energy governed by the liquid-drop model.

For the latter, the large K-value can be introduced by a displacement of the Fermi sphere in momentum space corresponding to the presence of a cranking constraint $-\omega_z j_z$ in the kinetic energy. The moment of inertia around a perpendicular axis can then be extracted as in ref. [3], which gives

$$\mathcal{J}^{\perp} = \mathcal{J}^{\perp}_{rigid} \left(1 + \delta \left(\omega_z/\omega_0\right)^2\right) \qquad (1.1)$$

where

$$\hbar\omega_0 = (\hbar^2/M)\, A^{-1/3} \approx 41\, A^{-1/3} \ \text{MeV} \qquad (1.2)$$

and the coefficient δ is about 0.1 for spherical and near-spherical shapes. The largest values of ω_z, which would still correspond to realistic K-values in nuclei, are an order of magnitude smaller than ω_0. Thus the rotational moment of inertia in the Fermi-gas model stays close to the rigid-body value even under the most rapid rotation around another axis that a nuclear system could hold. The latter rotation may of course induce deformation changes [4] and thereby influence the rigid-body value itself.

The RPA formalism of section 2.1 below has been suggested to us by Bohr and Mottelson [5] as a theoretical tool for analysing the deviations from this behaviour in the nuclei where there are yrast states of single-particle character at very high spins. The formalism starts from the K-scheme for single-particle spin alignment along a symmetry axis in the deformed shell model [2], and a collective rotation around a perpendicular axis will be found among the solutions of the RPA equations if it exists at all. The energy, or moment of inertia, and the collective enhancement of the in-band E2 transitions for such a mode can then be extracted according to a correspondence with the rotational model which is clarified in section 2.2. An even more essential characteristic of a collective band, which is arbitrarily imposed in the rotational model, is the presence of several, regularly spaced band members. A way of actually calculating irregularities in the energy spacing from the RPA formalism is briefly outlined in sect. 2.3, while a more readily obtainable quantity expressing the repeatability of the rotational excitations is introduced and discussed in sect. 2.4.

Experimental information could be obtained for example from the angular distributions [6] or the transition-energy correlations [7] of continuum gamma rays, or simply from discrete-line spectroscopy in appropriate nuclei [8]. A comprehensive theoretical survey over all the relevant regions of nuclei [9] lies beyond the scope of the present paper, and in particular the results of calculations for the A~150 region will be deferred to a forthcoming publication [10]. In section 3 below detailed

numerical results are given for two nuclei, ^{176}Hf and ^{212}Rn. They are selected because each is known from experiment [8,11] to represent a clearcut example of a characteristic situation [9], where single-particle rotation around a symmetry axis prevails along the yrast line at very high spin. Therefore it may be possible to draw some general conclusions from the calculations about the evolution of the collective mode with increasing single-particle angular momentum.

2. THE MODEL

2.1 The RPA formalism

Rotation around the 1-axis induces a change in the nuclear field [5], to first order

$$H' = -\alpha_1 \frac{\partial V}{\partial \varphi_1} \tag{2.1}$$

Let us associate a field operator F_1 with this variation:

$$F_1 = -\frac{1}{\kappa} \frac{\partial V}{\partial \varphi_1} \tag{2.2}$$

so that

$$H' = \kappa \alpha_1 F_1 \tag{2.3}$$

can be thought of as a linearisation of a two-body interaction

$$H_2' = \frac{1}{2} \kappa F_1^2 \tag{2.4}$$

The choice of the coupling constant will be given some attention (cf. below). A self-consistent value is obtained by requiring the amplitude

α_1 to be given by the self-consistency condition

$$\int \delta\rho \, F_1 \, d\tau = \alpha_1 \tag{2.5}$$

where $\delta\rho$ is the change of nuclear density incurred by the rotation,

$$\delta\rho = - \frac{\partial \rho_0}{\partial \varphi_1} \alpha_1 \tag{2.6}$$

From this it is obtained that

$$\varkappa = - A \left\langle \frac{\partial^2 V}{\partial \varphi_1^2} \right\rangle \tag{2.7}$$

With two modes ,rotation around the 1- and 2-axes, and transformation to spherical components, we obtain

$$H' = \varkappa (\alpha_1 F_1 + \alpha_2 F_2) = \tfrac{1}{2} \varkappa (\alpha^* F + \alpha F^\dagger) \tag{2.8}$$

and the corresponding two-body interaction

$$H_2' = \tfrac{1}{4} \varkappa (F F^\dagger + F^\dagger F) \tag{2.9}$$

Here α and F are the spherical components, and the field operator F can be written

$$F = - \frac{1}{\varkappa} i [J_+, H_0] \tag{2.10}$$

Since the major contribution to the commutator arises from an axially symmetric quadrupole field in H_0, the operator F contains a leading order term proportional to Y_{21}.

The Hamiltonian

$$H = H_0 + \tfrac{1}{4}\kappa \left(\tilde{F} F^{\dagger} + F^{\dagger} F \right) \tag{2.11}$$

is to be treated in the random phase approximation. The interaction is separable, though into non-Hermitian fields. When the starting point is a state with a non-zero K-value , the formalism and its physical interpretation [5] as presented below thus become somewhat different from the case when K is equal to zero, considered earlier by Hamamoto [12]. Some of the features of RPA on a K≠0 state are familiar from earlier work on gamma vibrations [13,14], where the symmetry of the field is Y_{22} instead of Y_{21}.

Here the operators

$$A^{\dagger}_{i+} \; , \; A^{\dagger}_{i-}$$

are introduced as creation operators for particle-hole states with $\Delta K=+1$ and $\Delta K=-1$ respectively, and

$$A^{\dagger}_{a+} \; , \; A^{\dagger}_{a-}$$

stand for the corresponding RPA phonon creation operators. The following standard relations are imposed

$$A^{\dagger}_{a+} = \Sigma_{i+} X_{a+,i+} A^{\dagger}_{i+} + \Sigma_{i-} Y_{a+,i-} A_{i-} \tag{2.12}$$

$$A^{\dagger}_{a-} = \Sigma_{i-} X_{a-,i-} A^{\dagger}_{i-} + \Sigma_{i+} Y_{a-,i+} A_{i+} \tag{2.13}$$

$$F = \Sigma_{i+} F_{i+} A^{\dagger}_{i+} + \Sigma_{i-} F_{i-} A_{i-}$$

$$= \Sigma_{a+} F_{a+} A^{\dagger}_{a+} + \Sigma_{a-} F_{a-} A_{a-} \tag{2.14}$$

$$[H_c, A^{\dagger}_{i\pm}] = \hbar\omega_{i\pm} A^{\dagger}_{i\pm} \tag{2.15}$$

$$[H, A^{\dagger}_{a\pm}] = \hbar\omega_{a\pm} A^{\dagger}_{a\pm} \tag{2.16}$$

The frequencies $\hbar\omega_{i\pm}$ are the unperturbed particle-hole excitation energies and $\hbar\omega_{a\pm}$ are the RPA roots. When pairing is included, the quantities $\omega_{i\pm}$ are reinterpreted as a difference between multi-quasiparticle energies. In general, the $\Delta v=0$ excitations are most important, and the corresponding energies $\omega_{i\pm}$ are of the form $\pm(E_\mu - E_\nu)$. The operators $A^{+}_{i\pm}$ also create $\Delta v=2$quasiparticle excitations. The strengths $F_{i\pm}$ are to be multiplied with the appropriate pairing factor: for $\Delta v=0$ and 2 the factors are $(U_\mu U_\nu - V_\mu V_\nu)$ and $(U_\mu V_\nu + V_\mu U_\nu)$ respectively. The sign inside the pairing factor reflects the even time-reversal character of the operators F and F^+, viz. they fulfill

$$\mathcal{T} F \mathcal{T}^{-1} = \tau F^{\dagger} \tag{2.17}$$

with a time-reversal quantum number $\tau=+1$.

The separability of the RPA relations allows the simplification into the equation

$$G(\omega_a) = \frac{1}{\kappa} \tag{2.18}$$

where

$$G(z) = \frac{1}{2} \sum_{i+} \frac{|F_{i+}|^2}{z - \omega_{i+}} + \frac{1}{2} \sum_{i-} \frac{|F_{i-}|^2}{-z - \omega_{i-}} \tag{2.19}$$

In addition, another equation is obtained by substituting ω_{i+} and ω_{i-} by their negatives yielding a dispersion function which is the mirror image of (2.19) and thus RPA roots which are the negatives of the solutions to (2.18).

The normalisation conditions are

$$\sum_{i+} |X_{a+,i+}|^2 - \sum_{i-} |Y_{a+,i-}|^2 = \pm 1 \qquad (2.20)$$

$$\sum_{i-} |X_{a-,i-}|^2 - \sum_{i+} |Y_{a-,i+}|^2 = \pm 1 \qquad (2.21)$$

for the a+ and a- roots respectively. The plus signs of the right hand side are valid for so-called physical roots and the minus sign for unphysical roots. Eq. (2.18) gives the physical a+ roots, which are all positive, and the unphysical a- roots, of which some may be positive, but most of them are negative.

A realistic example of a plot of G(z) is shown in fig. 1, obtained from the numerical calculations for the nucleus ^{176}Hf at K=14 in section 3 below. The figure illustrates the situation that is typical for a deformed nucleus. Note that the lowest physical root $\omega_{a=1+}$ does not lie close to any pole, which is one of the characteristics of a collective solution. The $\Delta K=\pm 1$ single-particle excitations with energies $\omega_{i\pm}$, corresponding to the poles in fig. 1, are marked out in fig. 2. There the tilted line is the Fermi level of the non-collectively rotating system [1,2]. The slope corresponds to the rotational frequency ω_{rot}. Only those single-particle transitions across the Fermi level are indicated which have non-zero matrix elements of the fields $F^+ \sim Y_{2-1}$ or $F \sim Y_{21}$ and also low enough energies to be seen in fig. 1.

From the condition

$$-\hbar\omega_{i'-} \leqq \hbar\omega_{rot} \leqq \hbar\omega_{i+}$$

it follows that the physical a+ roots and unphysical a- roots are well separated in eq. (2.18), i.e.

$$-\hbar\omega_{a'-} < \hbar\omega_{a+} \quad , \quad \text{all } a, a'$$

(the symbol $\hbar\omega_a$ always denotes a physical root). A solution $\omega_a=0$ is to be expected. It corresponds to a mode that simply changes the M quantum number, i.e. it produces a reorientation of the system as a whole.

The test for such a zero root is made by evaluating G(0). Using eqs. (2.2), (2.10) and (2.19) the dispersion relation yields

$$G(0) = -\frac{1}{2}\,\frac{1}{\kappa^2}\left\langle \frac{\partial^2 V}{\partial \varphi_1^2} + \frac{\partial^2 V}{\partial \varphi_2^2} \right\rangle \qquad (2.22)$$

and thus

$$G(0) = \frac{1}{\kappa} \qquad (2.23)$$

if the self-consistent value (2.7) of κ is used. Actually in the calculations below, the operator F is approximated by r^2Y_{21}, which is not exactly equal to the F of eq. (2.10) if P_4 distortions are included and if the $\bar{\ell}\cdot\bar{s}$ and $\bar{\ell}^2$ terms are defined in a stretched basis. Furthermore, the particle-hole excitations with energies ω_i>10 MeV are not taken into account explicitly. The corresponding terms in eqs. (2.18)-(2.20) are roughly constant at the comparatively small energies z where the interesting roots are to be found, so they can be thought to have been moved to the right-hand side of eq. (2.18) and absorbed into the coupling constant κ. This changes the selfconsistent value of κ by a factor of about two. In the practical calculations it is a great simplification to assume that the effective coupling constant κ can be <u>determined</u> from eq. (2.23).

The norm of the ω=0 solution is found to be

$$|F_{\alpha-}^{(0)}|^2 = \frac{1}{2K} \qquad (2.24)$$

assuming that a zero root is obtained from the mirror image of (2.17):

$$-G(-\omega_\alpha) = \frac{1}{\kappa}$$

whereas (2.17) would yield a negative value of the norm. Thus the

reorientation mode is one of the a- roots. It is the lowest of the physical a- roots unless there exists a $\Delta K=-1$ particle-hole state with a negative frequency $\hbar\omega_{i-}$.

The creation operator for the $\omega_{a-}=0$ mode is

$$A^{\dagger}_{a-}(0) = i\, F^{(0)}_{a-}\, J_- \tag{2.25}$$

and thus, as expected, it simply generates a change of the M quantum number.

For $K\neq 0$ the field F is non-Hermitian, whence the function G(z) in eq. (2.18) is asymmetric in z. Thus there are no normalisation problems as when K is zero. In the latter case the occurrence of a zero root is related to the transition to an unstable regime with an imaginary root [12].

The lowest a+ root can be a rotational excitation $(I=K) \rightarrow (I=K+1)$. In fact, to second order in ω_{a+} we have

$$\omega_{a+} = \frac{K}{\mathcal{J}} \tag{2.26}$$

where $\vec{\mathcal{J}}$ is the cranking moment of inertia:

$$\frac{2\mathcal{J}}{\hbar^2} = \sum_{i+} \frac{|(J_+)_i|^2}{\omega_{i+}} + \sum_{i-} \frac{|(J_-)_i|^2}{\omega_{i-}} \tag{2.27}$$

This is seen by expanding $G(\omega_{a+})$ around $\omega_{a+}=0$

$$G(\omega_{a+}) \approx G(0) + \omega_{a+} G'(0) + \tfrac{1}{2}\omega^2_{a+} G''(0) \tag{2.28}$$

and since $G(\omega_{a+}) = G(0) = \frac{1}{\ldots}$

$$\omega_{a+}\, G'(0) + \tfrac{1}{2}\, \omega_{a+}^{2}\, G''(0) = 0 \qquad (2.29)$$

from which eq. (2.26) follows.

The normalisation (2.20) yields

$$|F_{a+}^{(c)}|^2 = \frac{1}{2K} \qquad (2.30)$$

in the same approximation.

For more complete numerical results eq. (2.18) is to be solved rather than (2.29). Whereas eq. (2.29) produces only one non-zero root, acquiring the total strength, the lowest ω_{a+} root of (2.18) may be less collective. Though no negative physical a+ root can exist, there may be a non-collective lowest root corresponding to a $\Delta K=\pm 1$ state of single-particle character. Such a situation occurs if the field coupling to the lowest particle-hole state of $\Delta K=+1$ is very weak. In intermediate cases such a weak low-lying pole may cause a fragmentation of the collective mode. The mechanism for such poles will be seen in sect. 3.2 below.

2.2 Connections with the rotational model

The RPA formalism derived in the previous section is based on the assumption that the first excited state $|I+1,K\rangle_{I=K}$ in a rotational band, built on the highly aligned band head $|IK\rangle_{I=K}$, can be represented by means of $\Delta K=\pm 1$ vibrational phonons. We shall now attempt to discuss briefly the plausibility of this assumption.

As is well known, the properties of vibrational spectra differ essentially from those of rotational ones. The energy increases linearly with angular momentum I in the pure vibrational spectrum, and the only enhanced electromagnetic E2 transitions are those with a change in number of phonons n by one unit ($\Delta n=1$). On the other hand, a rotational spectrum exhibits a quadratic dependence of energy on I, and there are enhanced E2 transitions with both $\Delta I=1$ and $\Delta I=2$.

In spite of the essential differences between the properties in the two kinds of spectra, one may attempt to draw some analogies. This turns out to be possible for the first few states in the band in the case when there is a substantial aligned angular momentum K(K>>1). In this case, the transition energies between the neighbouring members in the band $|IK\rangle_{I=K}$, $|I+1,K\rangle$, $|I+2,K\rangle$ ... differ by an amount which is almost negligible compared to the total magnitude of the transition energy. In an ideal rotational band the transition energy between two neighbouring states with angular momenta (I+n) and (I+n-1) is

$$\bar{E}_{I+n} - \bar{E}_{I+n-1} = \frac{\hbar^2}{2\mathcal{J}} 2(I+n) \qquad (2.31)$$

whose relative variation with n is slow if I>>n. Thus the energy of the RPA phonon, which was seen above in eq. (2.26) to correspond to the cranking value for the lowest transition in the band, is also a reasonable approximation for the first few transitions.

Similarly, the unstretched reduced transition probability B(E2;I+n,K→I+n-1,K) for a rotor is proportional to the square of the vector addition coefficient $\langle I+n,K,2,0|I+n-1,K\rangle$, which can be shown to be n times stronger than B(E2;I+1,K→I,K) in the limit I>>n:

$$\left.\frac{B(E2;\, I+n, K \to I+n-1, K)}{B(E2;\, I+1, K \to I, K)}\right|_{K=I} = \frac{\langle I+n\ I\ 2\ 0 \mid I+n-1\ I\rangle^2}{\langle I+1\ I\ 2\ 0 \mid I\ I\rangle^2} \approx \frac{(3n/I)}{(3/I)} = n \qquad (2.32)$$

In the case of a vibrational spectrum, where n means the number of phonons we obtain again the same result

$$\frac{B(E2;\, n \to n-1)}{B(E2;\, 1 \to 0)} = n \qquad (2.33)$$

Furthermore, the stretched E2 transitions, forbidden in a vibrational spectrum because they change the number of phonons n by two units, come out to be strongly retarded in a rotational spectrum as well. Indeed, the

ratio of the stretched to nonstretched E2 transition rates in the case of an ideal rotor can be estimated in the following way

$$\left.\frac{B(E2;\, I+n, K \to I+n-2, K)}{B(E2;\, I+n, K \to I+n-1, K)}\right|_{K=I} = \frac{\langle I+n\ I\ 2\ 0 | I+n-2\ I\rangle^2}{\langle I+n\ I\ 2\ 0 | I+n-1\ I\rangle^2} = \frac{n-1}{2I} \tag{2.34}$$

This quantity becomes very small for I>>n.

The absolute scale of the E2 transitions in the rotational model are determined by the intrinsic quadrupole moment Q_0, and in particular the reorientation matrix element of the I=K band head gives

$$B(E2;\, I=K, K \to K, K) = \frac{5}{16}\frac{e^2}{\pi} Q_0^2 \langle KK\ 2\ 0 | KK\rangle^2 \approx \frac{5}{16\pi} e^2 Q_0^2 \tag{2.35}$$

The corresponding B(E2) for the correlated RPA band head can be obtained from the quadrupole matrix element between the band head and the zero-frequency reorientation mode by the definition

$$B(E2;\, I=K \to K) = e_{eff}^2 \left| \langle \omega=0 | r^2 Y_{2-1} | \tilde{0}\rangle \Big/ \langle I=K\ M=K\ \ 2\ -1 \,|\, I=K\ M=K\rangle \right|^2 \tag{2.36}$$

For any numerical solution it is straightforward to evaluate the matrix element. Furthermore, when the quadrupole operator is proportional to the field F, this matrix element must be proportional to $K^{-1/2}$ according to the exact result (2.24). Since the vector coupling coefficient in eq. (2.36) is also proportional to $K^{-1/2}$ for large K, the B(E2) value for reorientation contains no explicit K-dependence, just as in the rotational case. Employing the selfconsistent value of κ, it can be shown that the right hand side of eq. (2.36) does indeed contain Q_0 in the same way as eq. (2.35).

Ratios between transition rates in the band were given in eqs. (2.32) and (2.33). Let us finally check the B(E2) ratio between the lowest transition and the reorientation model. In the rotational model it is

$$\left| \frac{\langle K+1\ K\ 2\ 0 \mid K\ K\rangle}{\langle K\ K\ 2\ 0 \mid K\ K\rangle} \right|^2 \approx \frac{3}{K} \quad , \text{ large } K \tag{2.37}$$

Taking the approximate RPA solution from eq. (2.29), the transition and reorientation quadrupole matrix elements cancel in the ratio according to eqs. (2.24) and (2.30), and the remaining geometrical factors give

$$\frac{2K+1}{2K+3} \left| \frac{\langle K+1\ K\ 2\ 0 \mid K\ K\rangle}{\langle K\ K\ 2\ 0 \mid K\ K\rangle} \right|^2 \approx \frac{3}{K} \quad , \text{ large } K \tag{2.38}$$

i.e. the same result as in eq. (2.37) above.

In summary, we can see that the two possible ways of treating the collective excitation spectrum on the state $|Ik\rangle_{I-k}$, either as a rotation, or a vibration, both lead to similar results in the first approximation. The correspondence is shown pictorially in fig. 3.

2.3 A schematic model and higher order corrections

Higher order corrections to the RPA results, and the explicit calculation of quantities involving the multiphonon excited states, can be calculated with methods of nuclear field theory outlined in refs.[5,15]. Actually, we have found that very good collectivity is needed in order for the corrections to achieve improvements when only the next higher order terms beyond RPA are included. In the present subsection we shall therefore concentrate upon a simple model that yields some qualitative results on the correction terms, and on the multiphonon excitations to be discussed in the next subsection. The first anharmonic correction contributing to the energy of the second excited state in the band, or the two phonon states, is given by the diagrams shown in fig. 4. There the vertices 1, 2, 3, 4, 6 and 7 are determined by the RPA, while vertices 5 and 8 are connected with the particle-particle or hole-hole matrix elements of the interaction. The vertices with only one phonon a+ are shown in fig. 5, to which the hermitian conjugates should be added. The expressions for the four vertices shown in fig. 5 are

$$\Lambda_{(A)} = \kappa F_{i+}^{+} F_{a+}$$
$$\Lambda_{(B)} = \kappa F_{i-} F_{a+} \qquad (2.39)$$
$$\Lambda_{(C)} = \kappa F_{ki}^{+} F_{a+}$$
$$\Lambda_{(D)} = -\kappa F_{nm} F_{a+}$$

The magnitude of these vertices and the magnitude of the two-phonon energy-corrections corresponding to diagrams shown in fig. 4 can be estimated in a simple model where there are Ω_- degenerate $\Delta K=-1$ excitations of energy ε_- and Ω_+ degenerate $\Delta K=+1$ excitations of energy ε_+. The matrix elements have the same value: $F_{i-}=F_-$, for all the transitions ε_-, while $F_{i+}=F_+$ for the excitations ε_+. The graphical solution of the RPA equation (2.18) is illustrated in fig. 6. The energy ω of the collective state can be given in a simple closed form

$$\omega = \varepsilon_+ \frac{\alpha^2 - \beta^2}{\alpha^2 + \beta} \qquad (2.40)$$

where

$$\beta = \varepsilon_- / \varepsilon_+ \qquad (2.41)$$

and

$$\alpha = \left| \frac{F_-^2 \Omega_-}{F_+^2 \Omega_+} \right|^{1/2}$$

Expressions for the strength of vertices $\Lambda_{(A)}$, $\Lambda_{(B)}$, $\Lambda_{(C)}$ and $\Lambda_{(D)}$ of fig. 5 and eq. (2.39) can be obtained, for example

$$\Lambda_{(A)} = \frac{\beta}{\beta^2 + \kappa} \quad \frac{\alpha(1+\beta)}{(\alpha^2-\beta^2)^{1/2}} \quad \frac{\varepsilon_+}{\Omega_+^{1/2}} \tag{2.42}$$

It appears that all the quantities Λ_j, with j=A, B, C or D, are inversely proportional to $\sqrt{\Omega_+}$. Consequently, they are small for large Ω_+ if the quantities α and β are of the order of unity and $\alpha \neq \beta$. The contribution to the diagrams indicated in fig. 4 turns out to be roughly of the order of

$$\delta \approx \frac{\prod_j \Lambda_j}{\varepsilon_+^3} \qquad (j = A, B, C, D) \tag{2.43}$$

This follows from the fact that the diagrams contain four vertices and three energy denominators. Consequently, the ratio of δ to the phonon energy is

$$\frac{\delta}{\omega} \approx \frac{\delta}{\varepsilon_+} \approx \frac{\prod_j \Lambda_j}{\varepsilon_+^4} \approx \Omega_+^{-2} \tag{2.44}$$

which is very small for $\Omega_+ >> 1$. In that case the two-phonon energy should lie close to 2ω, as expected.

A further correction is shown in fig. 7. The diagram illustrates a possible coupling between the one-phonon and two-phonon states which contributes to the transition matrix element between them. Because of conservation of angular momentum projection (K) the phonon in the final state carries angular momentum $\Delta K=2$. Thus the upper vertex is a coupling predominantly of type Y_{22} rather than Y_{21}, expressing the fact that all components of the quadrupole field should be considered at the same time in a more accurate treatment.

2.4 Repeatability and collectivity

A necessary condition for the establishment of a rotational band on the high-K state is that the RPA-phonon can be repeated many times. As the RPA-phonon consist of particle-hole excitations, cf. eq. (2.12), it follows from the Pauli-principle that each particle-hole pair can be exploited only once in the creation of the multi-phonon state. A phonon with good repeatability contains many X:s and Y:s contributing to the sum in (2.12). This implies that the Pauli-principle should not have much influence on the few-phonon state. On the other hand, if the phonon consists mainly of a single particle-hole pair the exclusion principle is crucial already for the two-phonon state.Therefore a measure of the boson-character of the RPA-phonon is needed. A simple recipe for such a measure is given below where a quantity n is defined whose deviation from unity expresses the loss of norm due to the Pauli-principle when the RPA-phonon is repeated.

First, let us note that for a boson with creation operator B^+ and annihilation operator B

$$[BB, B^+B^+] = 2(BB^+ + B^+B) \qquad (2.45)$$

Taking the expectation value of both sides of (2.45) in a state such that $\langle i|BB^+ + B^+B|i\rangle \neq 0$ gives

$$\frac{1}{2}\,\frac{\langle i|[BB, B^+B^+]|i\rangle}{\langle i|BB^+ + B^+B|i\rangle} = 1 \qquad (2.46)$$

Guided by this we calculate the corresponding quantity for the RPA-phonon

$$n_i = \frac{\langle 0|[A, A^+A^+]|0\rangle}{\langle 0|AA^+ + A^+A|0\rangle} \qquad (2.47)$$

which defines n_i. The normalisation relations (2.19) and (2.20) are satisfied if the expectation value of the commutator $[A,A^+]$ in the uncorrelated groundstate is set to unity:

$$\langle 0|[A, A^+]|0\rangle = 1 \qquad (2.48)$$

Taking this uncorrelated ground state $|0\rangle$ as the state $|i\rangle$ in (2.47), the quantity η_0 is found to be

$$\eta_0 = 1 - (\Sigma_{i+} X_{i+}^4 - \Sigma_{i-} Y_{i-}^4)/(\Sigma_{i+} X_{i+}^2 + \Sigma_{i-} Y_{i-}^2) \quad (2.49)$$

In deriving (2.49) we have used the normalisation condition (2.19) and taking the exclusion principle explicitly into account through the relations

$$(A_{i+}^\dagger)^2 |0\rangle = 0$$
$$(A_{i-}^\dagger)^2 |0\rangle = 0 \quad (2.50)$$

where A_{i+}^+ and A_{i-}^+ are creation operators of particle-hole pairs.

It is instructive to calculate η_0 in the two-pole model presented in the previous subsection. The result, in terms of the parameters introduced there, is

$$\eta_0 = 1 - \frac{1}{\alpha^4 - \beta^4} \left(\frac{\alpha^4}{\Omega_+} - \frac{\beta^4}{\Omega_-} \right) \quad (2.51)$$

where α and β can be assumed to vary slowly. Thus, if η_0 is close to unity the degeneracies Ω_+ and Ω_- are large. In this case the correction due to the exclusion principle plays a minor role since there are many different particle-hole pairs available for the creation of the two-phonon state. On the other hand, if Ω_+ and Ω_- are small the value of η_0 is close to zero.

Supported by the results of the two-pole model it can be said that if η_0 is close to unity the RPA-phonon can be repeated sufficiently many times for the establishment of a band while a value of η_0 close to zero means that the multi-phonon state will peter out quickly with an increasing number of phonons due to the Pauli-principle. The quantity η_0 will in the following be referred to as the repeatability.

The matrix element between the ground state and a one-phonon state is the most commonly used measure of the collectivity of the one-phonon state. A large collectivity indicates that there are many particle-hole pairs contributing to the transition. However, in the calculations it

turns out that there may be more than one state with a collectivity several times larger than the single-particle value. In such a case the additional information given by the repeatability helps to select the most appropriate phonon for generating the rotational band. An example encountered in the calculations of sect. 3.2 below for the nucleus ^{212}Rn is shown in figs. 8 and 9. In fig.8 two solutions are seen to have roughly the same collectivities whereas the repeatability is 0.04 for the solution with lowest energy and 0.85 for the other one. The origin of the difference can be seen in fig.9 which shows a plot of the X and Y amplitudes in the respective wave functions. While the 931 keV solution consists mainly of a single-neutron particle-hole excitation within the f5/2 shell the 4006 keV solution is built out of many particle-hole pairs, most of them n i13/2 - g9/2 and p h11/2 - h9/2. The 931 keV solution may also gain strength from the Y:s , i.e. the $\Delta K=-1$ amplitudes. A different case is shown in figs. 10 and 11. The response function of the well-deformed nucleus ^{176}Hf considered in sect. 3.1 below has a single pole somewhat below the others. The smooth overall distribution of poles makes it possible to have several solutions with good repeatability. Actually, the second root has larger repeatability, whereas the first one by far carries the most strength. Comparing the B(E2)-values of the two roots with the B(E2)- value of the reorientation mode, it is clear that the first root is the rotational one, though it has smaller repeatability than the second root due to a larger admixture of the lowest single-particle mode. Such an admixture cannot contribute to many rotational excitations, and higher up the band can be expected to lose its identity, or at any rate a substantial part of its moment of inertia.

3. CALCULATIONS AND RESULTS

The technique discussed in this paper is used to describe rotational motion around an axis perpendicular to the symmetry axis and on an equal footing with the true $\Delta K=1$ excitations, starting from a high K state. It is evident from the results that both exist and contribute to the spectrum calculated.

3.1 The nucleus ^{176}Hf

3.1.1 The experimental situation

The first archetype to be studied, ^{176}Hf, belongs to a class of stably deformed nuclei with large number of high-Ω Nilsson orbitals close to the Fermi level. Single-particle configurations with several Ω-contributions aligned to form a large total K may then become yrast. In ^{176}Hf several two-quasiparticle states of this type are observed near yrast [16], while a few four- and six-quasiparticle states are known to come below the ground-band levels of the same spin [8]. The latter situation is predicted to persist up to an angular momentum of about 40-50. In the terminology of refs.[1,2] it corresponds to rotation around the prolate symmetry axis, favoured in this case by special shell effects. Rotation around a perpendicular axis, which would be favoured for a prolate rigid body, gives rise to the collective ground band. Similar, collective bands are observed [8,16] on the K= 6, 8, 8', 14 and 16 levels, and presumably on many others up to very high spins. The energy spacings and branching ratios in these bands, which are the ones of interest in the present work, have not been seen to deviate appreciably from the rotational-model description, although the moment of inertia may differ a bit from one band to another. Consequently, in studying the high-K bands of ^{176}Hf with the formalism of section 2, we know a priori that this is a case where the collectivity should be fully developed, and at lower spins the numerical results can be checked against measured data. It is known from earlier cranking-model calculations[18] that the experimental moments of inertia are fairly well reproduced.

3.1.2 Details of the calculations

The RPA results below are based on the Nilsson potential at the equilibrium deformation for rotation around a symmetry axis [9,17] ε=0.25 and ε_4 = 0.04, which does not vary appreciably with the angular momentum. The same standard single-particle and pairing parameters as in refs.[9,17] are employed, and since the RPA coupling constant is determined by eq. (2.23) there are no further parameters. The matrix elements of the field operator F, that creates the ΔK=1-excitations, are proportional to the matrix elements of j_+, weighted by the single-particle energy difference (see eq.(2.10)), so the analogue of a decoupling factor is superficially eliminated, since the corresponding

matrix element is zero. For a harmonic oscillator the matrix elements of F are proportional to those of the operator r^2Y_{21} (see ref.[12]). First the single-particle energies and r^2Y_{21} matrix elements are calculated taking the stretching of the basis into account. Next the single-particle occupancies corresponding to the optimal states [12] are determined by tilting the Fermi level as indicated for K=14 in fig.2 above. There is a good consensus on the detailed configurations for the experimentally known high-K levels obtained in the present model [17] and from other considerations [8,16,18]. For a given configuration the energies and r^2Y_{21} matrix elements of the possible $\Delta K=\pm 1$ one-particle or quasiparticle rearrangements define the RPA response function. The low-energy part of the response function for K=14 is shown in the lower part of fig. 10. Energies greater than 10 MeV need not be taken into account explicitly, as discussed in sect. 2.1 above, since their effect is absorbed into the coupling constant given by eq. (2.23). The physical roots of the dispersion relation (2.18), which is represented graphically in fig. 1, are determined numerically with an accuracy of 0.0001 MeV. The result for K=14 is shown in the upper part of fig. 10. The energy is taken to define a moment of inertia according to (2.26),which may be more or less meaningful depending on the extent to which the excited state should be regarded as a member of a high-K rotational band or a dressed $\Delta K=1$ intrinsic excitation. It is straightforward to obtain the amplitudes X_{i+} of the $\Delta K=+1$ components and Y_{i-} of the $\Delta K=-1$ components shown in fig. 11 for the two lowest roots at K=14, and hence all the other quantities defined in sect. 2. The B(E2) values are calculated under the somewhat schematic assumption of an effective charge equal to unity for both protons and neutrons.

3.1.3 Results for ^{176}Hf

The first square in fig. 12 shows the equilibrium deformation ε_2 of each optimal high-K level, in this case a constant. The remaining squares contain information about the first excited RPA state based on each optimal state whose energy is represented as a moment of inertia $\mathcal{J}$. One measure of the collectivity is the B(E2) reduced transition rate from the excited state to the correlated band head, expressed in single-particle units [5], and another is the repeatability η_0 of the excitation. The aim of the present work is to study the connections relating these

quantities with each other and with the microscopic picture illustrated in figs. 2 and 10.

In a plot like fig. 2 the curvature of the bows, that connect the states originating from the same j-shell, follows the deformation in sign and magnitude. The curvature is large in the present well-deformed case. Therefore the lowest poles of the response function, which generally correspond to single-particle transitions within j-shells, have rather large energies. The response function for K=14 in the lower part of fig. 10 has only one strong pole in the 1-2 MeV range. Above 2 MeV there is a forest of poles extending up to about 7 MeV. The dense part between 2 and 3 MeV comes mainly from transitions within the valence j-shells, while the thicket at 5 MeV comes from transitions between shells like p $h_{11/2}$ and $f_{7/2}$, n $i_{13/2}$ and $g_{9/2}$. The upper part of fig. 10 shows how the RPA solutions tend to pick up some collectivity in the low-density parts of the response function, and especially this is the case for the lowest solution which comes in the energy gap below the lowest pole. However, as pointed out in sect. 2.4 and shown by eq. (2.38), this conventional measure of RPA collectivity contains a 1/K dependence which emerges as a purely geometrical factor in the rotational model. The numerical results in fig. 12 for the B(E2) value do indeed conform fairly well to the 1/K curve, also drawn in the figure. The systematic deviation is largely due to the hexadecapole term, which is neglected in the RPA field. Contrary to the B(E2) value, the repeatability r_0 is seen to stay almost constant, around 0.8, which shows that the collectivity character of the bands remains intact at the very highest spins. The repeatability even increases a bit in going from K=14 to 22, because the lowest pole in the response function (fig. 10) corresponding to a transition within the $i_{13/2}$ shell is then blocked out. In terms of fig. 2 the Fermi level is tilted so that it no longer intersects the $i_{13/2}$ bow at the low-energy transition marked D.

The same mechanism that leads to this <u>increase</u> of the repeatability also leads to a substantial <u>decrease</u> in the rotational moment of inertia seen in fig. 12 between K=14 and 22. There are no more low-energy poles, and at higher K-values the moment of inertia stays about constant.

For lower K also the experimental moments of inertia are marked out by crosses in fig. 12. The theoretical value for the K=0 ground band, which comes only slightly below the experimental values, was obtained in ref. [19] by cranking the Nilsson potential at the relevant deformation.

It is indicated by an open circle in fig. 12. The calculated moments of inertia for K=8 and 14, within the region of the pairing collapse [17], also come slightly below the experimental values but exhibit the correct trend. For K=8 results are shown for two bands, one with two neutron quasiparticles and one with two proton quasiparticles. The observed difference between their moments of inertia is correctly reproduced. Despite the collapse of pairing, the moment of inertia decreases in going to K=22, due to the blocking of the low-energy poles exemplified above. In the absence of low-energy poles neither the moment of inertia nor the other properties depend very sensitively on the presence or absence of pairing. This is demonstrated by the results in table I, obtained for K=14 by varying the pairing gap as though it were a free parameter.

Finally it may be noted that the moment of inertia does not come anywhere near the rigid-body value, marked by the dot-dashed line in fig. 12, contrary to the result (1.1) of the Fermi gas model. The physical implication is shown in fig. 13. At low spins, pairing correlations affect the slope of the solid curve representing the ground band, and the slope of the dashed curve connecting the lowest high-K levels, with the result that they become about the same as the slope of the straight lines representing the high-K bands. Therefore the latter may help to conduct a gamma cascade roughly parallel to the yrast line, characterised by $\Delta I=1$ M1/E2 transitions [6,8]. For high K-values, the moment of inertia for the continuation of the K=0 ground band, and also the effective moment of inertia for rotation around a symmetry axis, are of the same order of magnitude as for rigid-body rotation. The moment of inertia for the high-K bands, however, is roughly half as large. Nevertheless, they are predicted to be excellent rotational bands. Instead of carrying the cascade parallel to the yrast line, they could help to funnel it down rather rapidly into the high-K band heads. The numerical results, and our qualitative understanding of the response function, suggest that the very high-K bands may have similar moments of inertia and could therefore give rise to coherence effects in transition-energy correlation experiments.

3.2 The nucleus ^{212}Rn

Nuclei characterised by closed or nearly closed shells and spherical shape in the ground-state configuration, and particularly the nuclei in

the lead region, are generally expected to exhibit yrast rotation around a symmetry axis [2,7,20]. When there are a few particles outside the closed shells, as in $^{212}_{86}Rn_{126}$, the most favourable way of generating angular momentum is for the valence particles to align themselves in the orbitals of highest spin above the shell. Such orbitals are always oblate, and the valence configuration will also polarise the core to a small oblate deformation. Consequently, when core excitations are needed to increase the angular momentum still further, the most favoured ones involve spherical rather than oblate holes below the shell gap, and again oblate particle states above the gap, so the oblate deformation continues to increase with increasing angular momentum, just as for the rotating liquid drop. Comparison between theory [7,21] and experiment [11] indicates that this does indeed occur for the nucleus ^{212}Rn.

In the following we will investigate if the deformation caused by the spin-aligned orbitals also makes it possible for the nucleus to rotate collectively. There is no evidence for this in the discrete-line data [11], which extend up to angular momentum 30 where the calculated deformation is ε=-0.1. However, the deformation at spin 51 is predicted to be ε=-0.24, ε_4=0.04, which is as large as in ^{176}Hf. In the calculations we use the DMO single-particle parameters employed for the description of ^{212}Rn in ref. [7].

It was seen above in connection with fig. 8 that even at the very small deformation of a state with spin below 30, there appears an RPA solution which has the repeatability characteristic of a good collective rotational mode. It lies at high energy, about 4 MeV above the band head and just below the energies of the single-particle excitations across the shell gap which build it up. The increase of the deformation of the optimal states with K can be followed in the upper lefthand section of fig. 14. This figure is constructed in complete analogy with fig. 12 for ^{176}Hf except that the excited state marked out for each optimal K is the lowest state only for $K \geq 30$. The others are selected because they are best qualified to represent a collective rotation by having an enhanced B(E2) and good repeatability. The calculated evolution of the band properties are shown in the other three sections. For K=48 and 51 there are three equally good candidates (c.f. the upper part of fig. 15) and all three are represented in fig. 14. Since ε_2 is roughly linear in K, it may be expected on the basis of the rotational model that the B(E2) goes as K^2, i.e. the square of the quadrupole moment, times the geometrical factor 1/K which governs the B(E2) in ^{176}Hf (fig. 12). Very

roughly, the B(E2) values for ^{212}Rn in fig. 14 conform to such a trend. For K-values around 50, where $|\varepsilon_2|$ in ^{212}Rn becomes as large as ε_2 in ^{176}Hf, the calculated B(E2) values in both cases lie around 5 single-particle units. However, the behaviour of ϑ and η_0 at large K reveal important differences between the two cases. Contrary to the situation in ^{176}Hf, the very high-K collective rotational RPA solutions for ^{212}Rn are fragmented by low-energy poles in the response function. The effect is seen in fig. 14 above K=30, where the repeatability of the lowest collective solution drops into the range $\sim$0.5 and the so-called moment of inertia, representing the inverse of the energy, increases in some cases almost up to the rigid-body value. In other cases the moment of inertia corresponding to the lowest solution is a somewhat smaller fraction of the rigid-body value than in ^{176}Hf.

The microscopic mechanisms can be deduced from the response function in the lower part of fig. 15, which may be compared with the response function for ^{176}Hf in fig. 10. First, the forest which in fig. 10 extends down to about 2 MeV begins to thin out at somewhat higher energy in ^{212}Rn. This may be regarded as a reminiscence of the closed shells. Certainly the deformation brings the occupied and unoccupied levels closer in energy, but not primarily the ones which differ by only one unit in Ω.

Secondly, in ^{212}Rn there may occur some poles scattered over the low-energy gap in the response function which fragment the collectivity. It may be noted for example in the upper part of fig. 15 that the collectivity is best in the RPA solutions with lowest energy, while the repeatability is best in the ones closest to the low-energy fringe of the forest. The lowest pole in fig. 15 corresponds to a single-particle transition between the Ω=-j orbitals of the proton $h_{9/2}$ and $f_{7/2}$ shells, and it must be regarded as an incidental item. In fact, the exact analogue of this transition in ^{176}Hf, but there for Ω=+j and neutrons, cand be understood from fig. 2 to give rise to a low-energy pole in the response function for all high-K configurations where one of the levels is occupied. The second low-lying pole in fig. 15 does, however, represent a systematic feature which makes fragmentation more likely to occur in oblate than in prolate nuclei. It corresponds to the transition between Ω=-9/2 and -7/2 within the proton $h_{9/2}$ shell, and again the analogue for neutrons and opposite sign on the Ω-values can be seen in fig. 2 to occur for ^{176}Hf. There, however, it comes 1 MeV higher in

energy and thus it is not a low-lying pole in for example figs. 1 and 10. The reason for the difference is the hexadecapole deformation, which is ε_4=0.04 in both cases. As can be seen for example in fig. 9 of ref. [22], the energy splitting between the two orbitals of highest Ω in a j-shell is reduced by a positive ε_4 in the oblate case but enlarged in the prolate case. Since positive ε_4 values are favoured by the liquid drop in both cases, this oblate-prolate asymmetry will tend to make fragmentation of the collective high-K bands more common in oblate nuclei.

The collective excitations calculated on the optimal yrast states in ^{212}Rn are represented schematically in fig. 16 by long, medium or short lines depending on the repeatability. The slope, corresponding to the inertia parameter, is generally much larger than the effective inertia parameter of the yrast line for those collective excitations that have good repeatability and consequently give rise to regular bands.

4. CONCLUSIONS

The random phase approximation is useful for a microscopic treatment of collective rotation in non-spherical nuclei. Wher the rotation is based on a high-K single-particle configuration the energy of a strongly collective RPA phonon can be identified with the cranking moment of inertia, and it is possible to draw a farreaching analogy with the rotational model. In addition, the RPA formalism is able to distinguish and describe the collective rotational mode in situations where there is competition or fragmentation from $\Delta K=1$ single-particle excitations of low energy.

Numerical calculations based on the Nilsson model description of the nuclei ^{176}Hf and ^{212}Rn indicate that collective rotation around an axis perpendicular to the axis of symmetry and spin alignment is a general consequence of deformation. However, contrary to the Fermi gas model the moment of inertia for the transverse mode does not assume the rigid-body value like the moment of inertia for the primary mode of rotation, i.e. around the symmetry axis. Therefore, in a plot of E vs. I the collective bands slope up rather steeply relative to the effective yrast line, contrary to what is observed in ^{176}Hf, where the respective slopes are almost equal. There a special situation arises from a conjunction of fragmentation, acting to reduce the energy of the lowest

transverse rotations, and pairing effects which tend to increase the slope of the yrast line at the relatively low spins involved. At higher spins, and preferentially in oblate nuclei, such favourable fragmentation may occur for the collective rotation based on several of the high-K levels.

We would like to thank Aage Bohr and Ben Mottelson, who have helped us with this paper dedicated to the memory of Sven Gösta Nilsson.

REFERENCES

1. A. Bohr and B.R. Mottelson, Phys. Scripta 10A (1974) 13.

2. G. Andersson, S.E. Larsson, G. Leander, P. Möller, S.G. Nilsson, I. Ragnarsson, S. Åberg, R. Bengtsson, J. Dudek, B. Nerlo-Pomorska, K. Pomorski and Z. Szymański, Nucl. Phys. A268 (1976) 205.

3. A. Bohr and B.R. Mottelscn, Nuclear Structure, vol. i(Benjamin, New York, 1975).

4. S. Cohen, F. Plasil and W.J. Swiatecki, Ann. of Phys. 82 (1974) 557.

5. A. Bohr and B.R. Mottelson, Nuclear Structure, vol. 2 (Benjamin, New York, 1975),
and informal notes, 1978.

6. J.O. Newton and S.H. Sie, Nucl. Phys. A334 (1980) 499.

7. O. Andersen, J.D. Garrett, G.B. Hagemann, B. Herskind, D.L. Hillis and L.L. Riedinger, Phys. Rev. Lett. 43 (1979) 687.

8. T.L. Khoo, F.M. Bernthal, R.G.H. Robertson and R.A. Warner, Phys. Rev. Lett. 37 (1976) 823.

9. C.G. Andersson, G. Hellström, G. Leander, I. Ragnarsson, S. Åberg, J. Krumlinde, S.G. Nilsson and Z. Szymański, Nucl. Phys. A309 (1978) 141.

10. C.G. Andersson, T. Bengtsson, R. Bengtsson, J. Krumlinde, G. Leander, P. Olanders, I. Ragnarsson, S. Åberg, K. Neergård and Z. Szymański, Proc. Nobel Symp. on nuclei at very high spin - Sven Gösta Nilsson in memoriam, Örenäs, June, 1980, to be published in Phys. Scripta.

11. D. Horn, O. Häusser, T. Faestermann, A.B. McDonald, T.K. Alexander, J.R. Beene and C.J. Herrlander, Phys. Rev. Lett. 39 (1977) 389.

12. I. Hamamoto, Nucl. Phys. A177 (1971) 484.

13. D.R. Bès and Cho-Yi-Chung, Nucl. Phys. 86 (1966) 581.

14. C.G. Andersson and J. Krumlinde, Nucl. Phys. A291 (1977) 21.

15. P.F. Bortignon, R.A. Broglia, D.R. Bès and R. Liotta, Phys. Rep. 30C (1977) 305.

16. T.L. Khoo, F.M. Bernthal, R.A. Warner, G.F. Bertsch and G. Hamilton, Phys. Rev. Lett. 35 (1975) 1256.

17. S. Åberg, Nucl. Phys. A306 (1978) 306.

18. A. Faessler and M. Ploszajczak, Phys. Rev. C16 (1977) 2032.

19. J. Krumlinde, Nucl. Phys. A121 (1968) 306.

20. T. Døssing, K. Neergård, K. Matsuyanagi and Hsi-Chen Chang, Phys. Rev. Lett. 39 (1977) 1395.

21. K. Matsuyanagi, T. Døssing and K. Neergård, Nucl. Phys. A307 (1978) 253.

22. S.E. Larsson, G. Leander and I. Ragnarsson, Nucl. Phys. A307 (1978) 189.

TABLE CAPTION

Table 1. The energy of the lowest solution, its B(E2)-value and its repeatability, n_0, for the nucleus ^{176}Hf, $K^{\pi}=14^{-}$, deformation $\varepsilon_2=0.25$ and $\varepsilon_4=0.04$. The proton and neutron pairing gaps are varied from the calculated ground-state values down to zero. The latter is the value obtained for K=14 from a blocked BCS calculation.

Table I

Δ_p (keV)	Δ_n (keV)	$\omega_{a=1+}$ (keV)	B(E2) (B_{sp})	n_o
874	737	453	45.5	0.88
699	510	425	44.6	0.84
524	442	389	44.2	0.79
370	295	354	43.7	0.73
175	147	327	43.5	0.68
0	0	316	43.5	0.68

FIGURE CAPTIONS

Fig. 1. A plot exemplifying a dispersion function $G(\omega)$, as defined in eq. (2.19), here for the case of excitations built on the $K^{\pi}=14^{-}$ state in ^{176}Hf. The quasiparticle poles are denoted by letters A to E consecutively from left to right. Here A, B and C are $\Delta K=-1$ annihilation modes and D and E are $\Delta K=+1$ creation modes. The deformation is $\varepsilon_2=0.25$, $\varepsilon_4=0.04$. The lowest positive root $\omega_{a=1+}$ is strongly collective, while the first negative root below the zero-frequency root is an example of a non-collective single-particle excitation.

Fig. 2. Single-particle levels in ^{176}Hf plotted vs energy and the Ω quantum number. Levels originating from the same j-shell are connected into bows. The transitions giving rise to the poles in fig. 1 are marked here with the corresponding letters A to E. The straight lines show the tilted Fermi surface that produces the optimal state $K^{\pi}=14^{-}$. Encircled signs denote single-particle states of indicated parity.

Fig. 3. A picturesque view of the mode under consideration and a comparison of the rotational model with the RPA results in the collective limit ($K>>0$).

Fig. 4. Examples of diagrams contributing to corrections to the 2-phonon excitations.

Fig. 5. Definition of the four different vertices A-D referred to in the text (eq. 2.39).

Fig. 6. A plot of the dispersion function $G(\omega)$ for the two-pole model (c.f. fig. 1).

Fig. 7. The diagram representing the coupling between the 2-phonon $\Delta K=1$ state and another kind of quadrupole phonon built out of $\Delta K=2$ excitations.

Fig. 8. The response function (lower part) and the solutions (upper part) of the RPA equation both plotted on the same scale for the nucleus ^{212}Rn, $K^{\pi}=23^{-}$, deformation $\varepsilon_2=-0.06$. Note that the strength after the RPA diagonalisation is mainly carried by two states at 931 keV and 4006 keV.

Fig. 9. The wavefunctions of the first and fifth root of the RPA equation for the case shown in fig. 8. The first root is seen to be mainly a particle-hole excitation, hence with low repeatability, whereas the fifth root has contributions from many $\Delta K=1$ transitions and consequently good repeatability.

Fig. 10. The reponse function (lower part) and the solutions (upper part) of the RPA equation for the nucleus ^{176}Hf, $K^{\pi}=14^{-}$, deformation $\varepsilon_2=0.25$ and $\varepsilon_4=0.04$. After the RPA diagonalisation most of the strength is carried by the 316 keV soltuion. Also the second solution, which lies above the isolated lowest pole, is somewhat more collective than the others.

Fig. 11. The wavefunctions of the first and second root of the RPA equation for the case shown in fig. 10. It is seen that the first root has greater collective enhancement of the E2 matrix element, while the second one has higher repeatability.

Fig. 12. Results of the calculations for the nucleus ^{176}Hf as described in sect. 3.1. The calculated quantities are shown as functions of the aligned angular momentum K. The two different K=8- states considered are labelled n and p. Crosses in the lower left plot denote experimental values and the circle at K=0 is the theoretical value of the moment of inertia from ref. [19]. The quantity η_0 is the repeatability, defined in sect. 2.4.

Fig. 13. An E versus I plot for the nucleus ^{176}Hf, deformation $\varepsilon_2=0.25$ and $\varepsilon_4=0.04$. The solid line corresponds to K~0 rotation around an axis perpendicual to the symmetry axis. The dashed line is for rotation around the prolate symmetry axis. Dots indicate individual high-K states and the straight lines emerging from these represent rotational bands with moments of inertia as given in fig. 12.

Fig. 14. Same as fig. 12, but for the spherical-oblate nucleus ^{212}Rn. The collective strength at spins 48 and 51 is distributed mainly over three solutions, all of which are shown in the plot.

Fig. 15. The response function (lower part) and the solution (upper part) of the RPA equation for the nucleus ^{212}Rn, $K^{\pi}=51^{+}$, deformation $\varepsilon_2=-0.24$ and $\varepsilon_4=0.04$. Due to the low-energy poles the strength is distributed over several RPA solutions.

Fig. 16. Same as fig. 13, but for the nucleus ^{212}Rn. The length of the lines at spin 23, 48 and 51 illustrate the repeatability of the respective solutions.

^{176}Hf

$K^{\pi}=14^{-}$

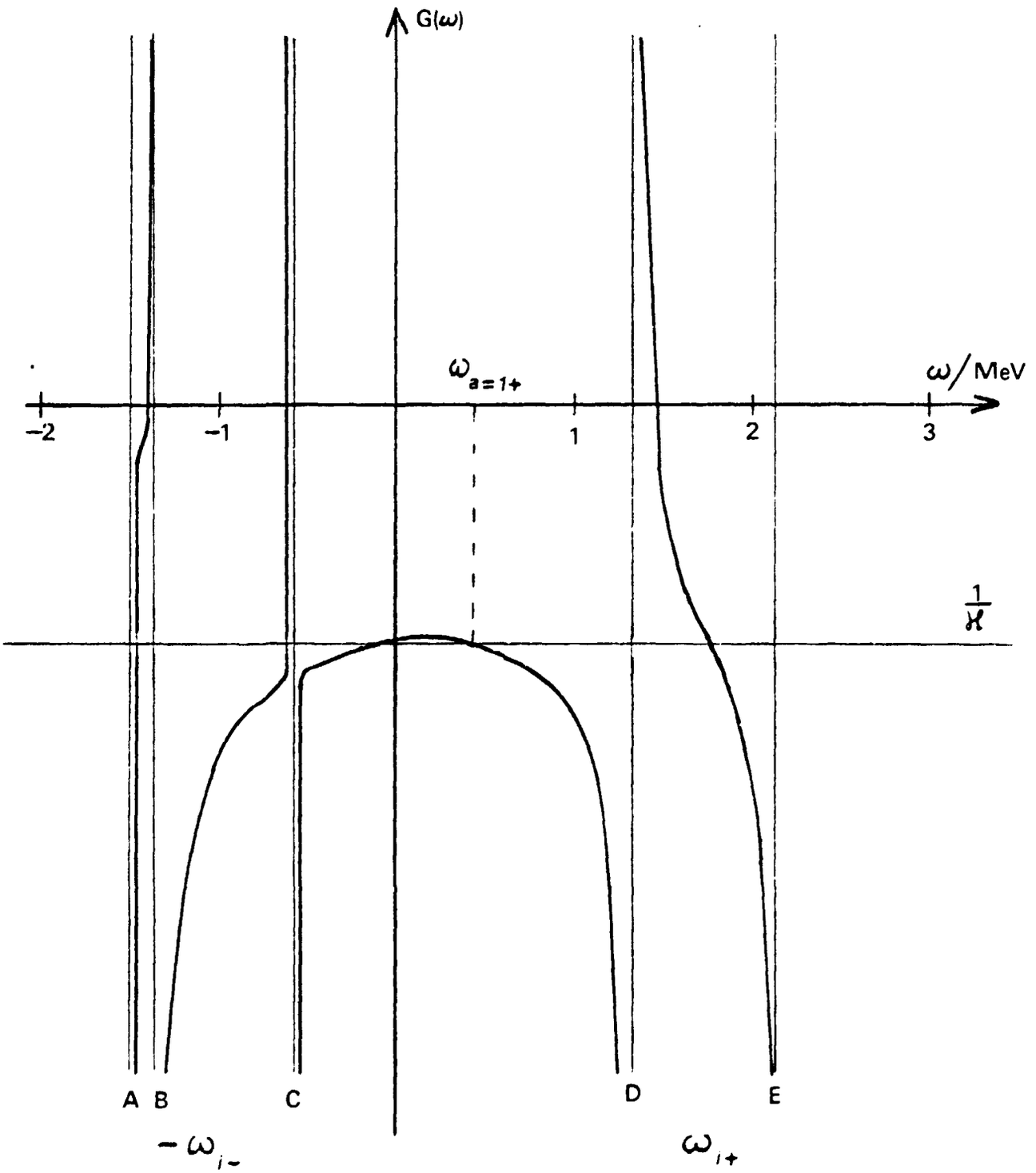

FIG. 1

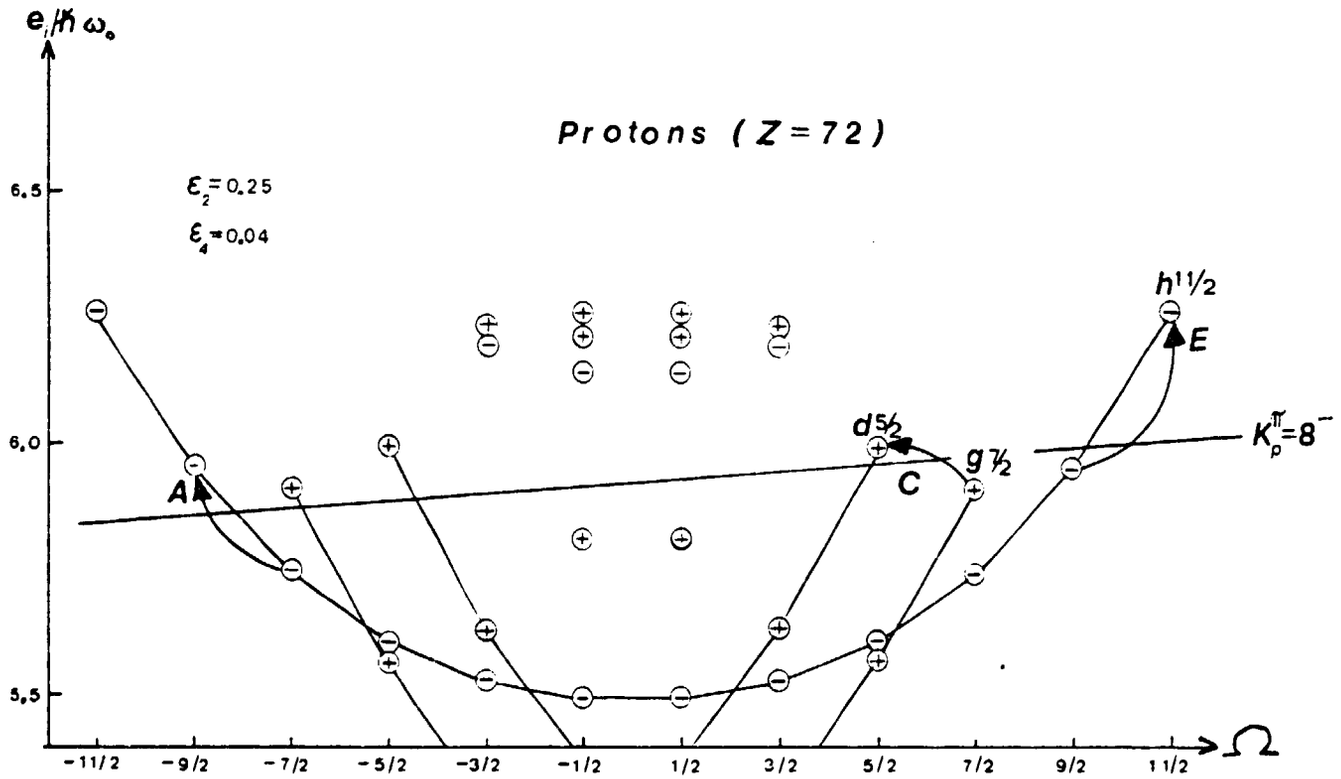
$e_i/\hbar\omega_0$
Protons (Z = 72)
$\varepsilon_2 = 0.25$
$\varepsilon_4 = 0.04$
6.5
6.0
5.5
$h^{11/2}$
E
$d^{5/2}$
$g^{7/2}$
C
A
$K_p^{\pi}=8^-$
-11/2 -9/2 -7/2 -5/2 -3/2 -1/2 1/2 3/2 5/2 7/2 9/2 11/2
Ω

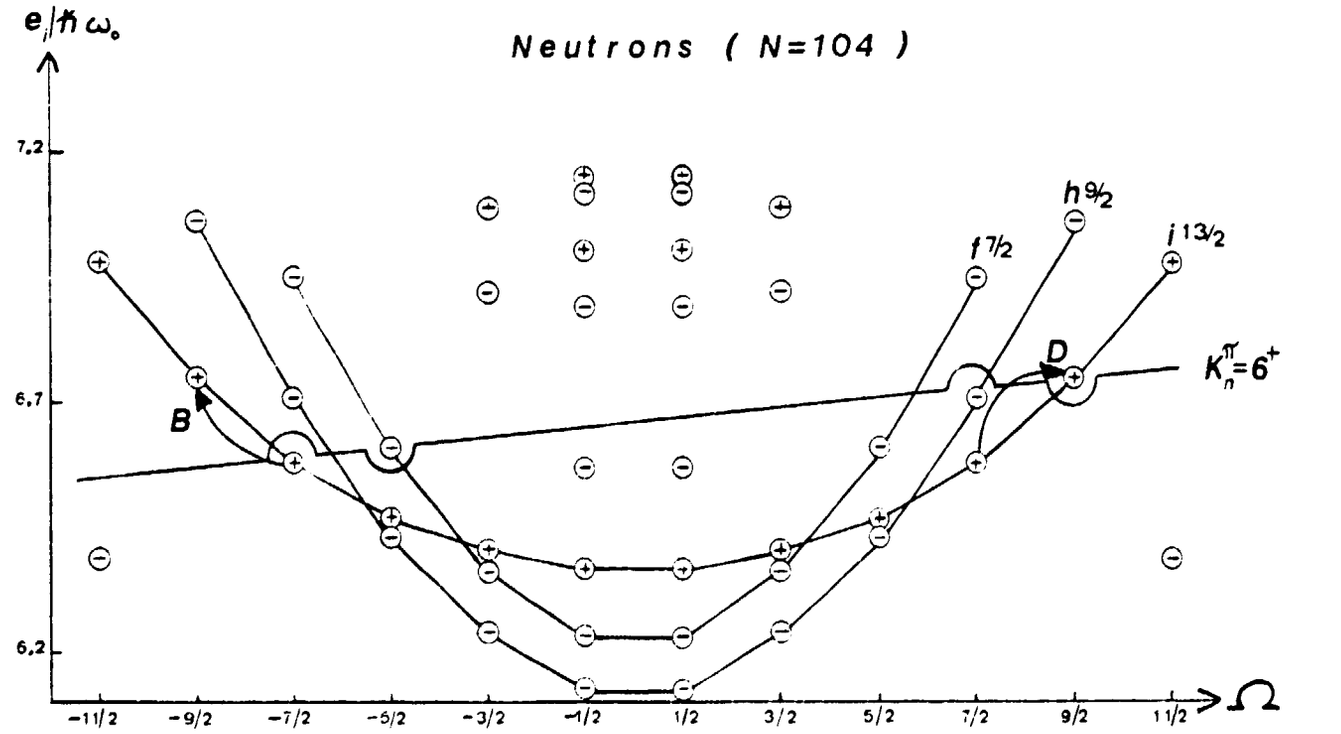
$e_i/\hbar\omega_0$
Neutrons (N=104)
7.2
6.7
6.2
$h^{9/2}$
$i^{13/2}$
$f^{7/2}$
D
$K_n^{\pi}=6^+$
B
-11/2 -9/2 -7/2 -5/2 -3/2 -1/2 1/2 3/2 5/2 7/2 9/2 11/2
Ω

FIG. 2

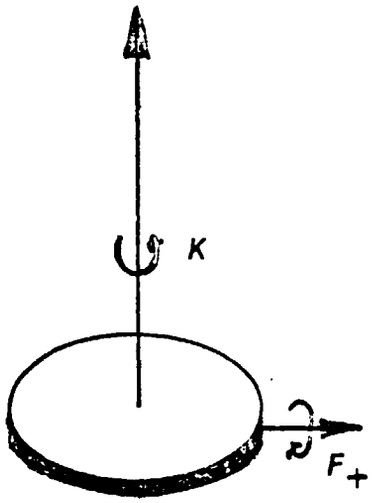

Rotational model **RPA-formalism**

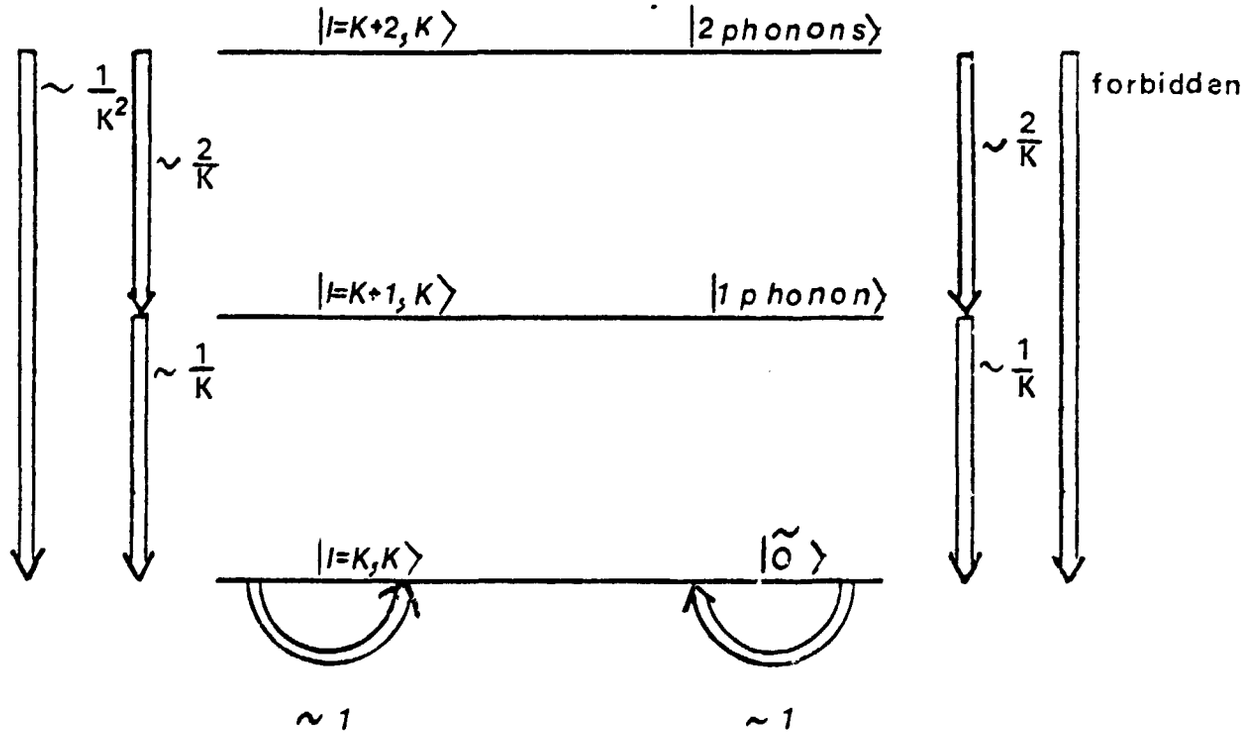

$K >> 0$

FIG. 3

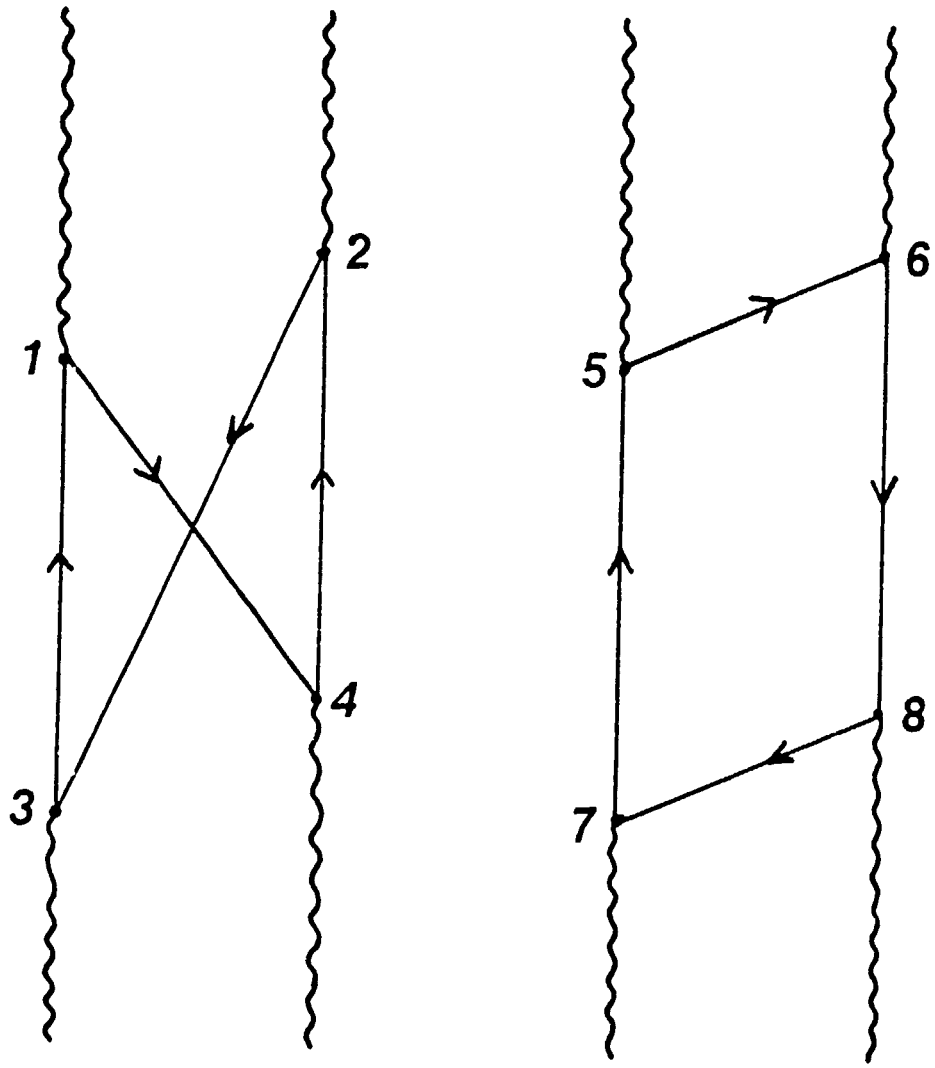

FIG. 4

FIG. 5

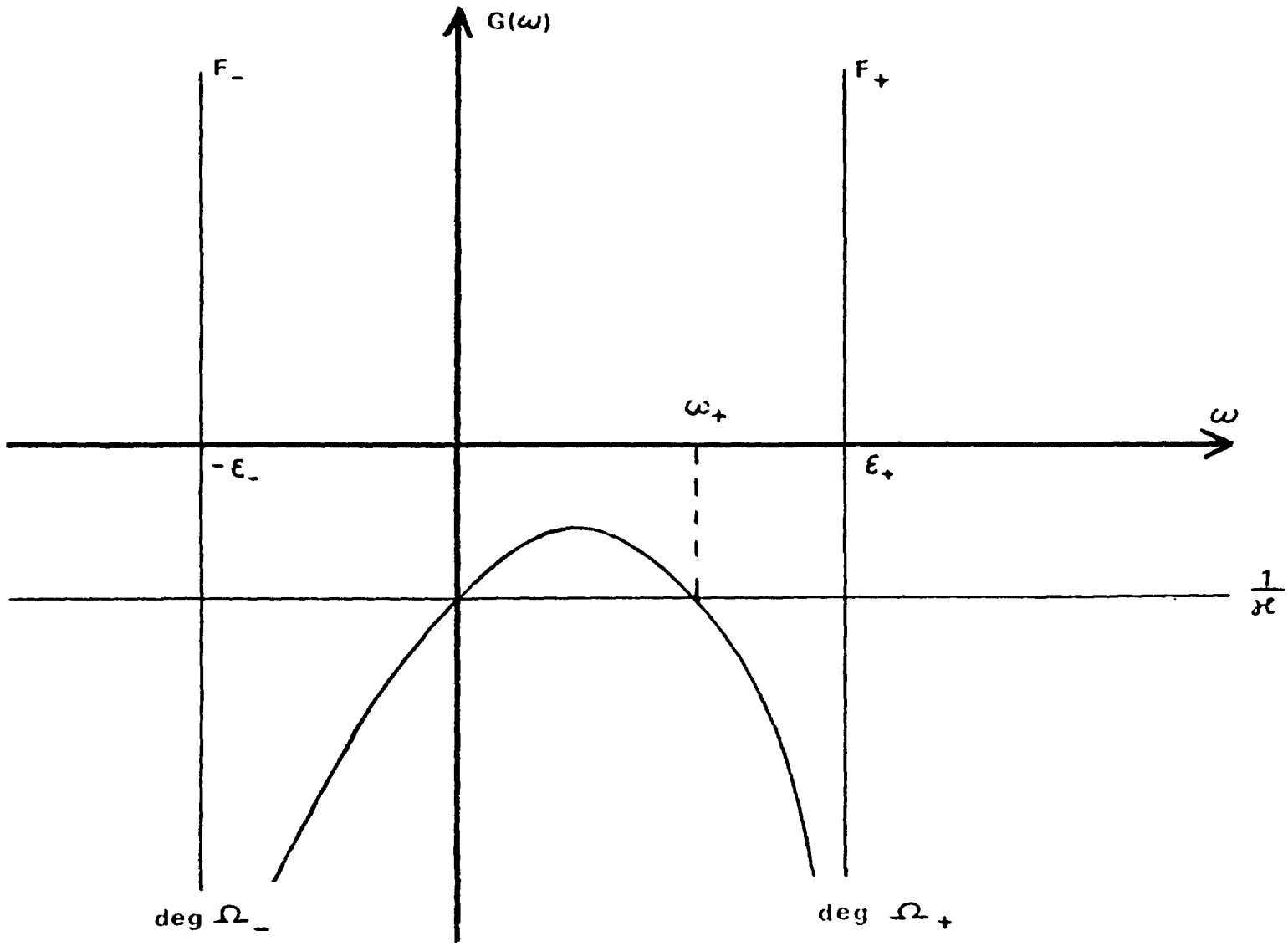

FIG. 6

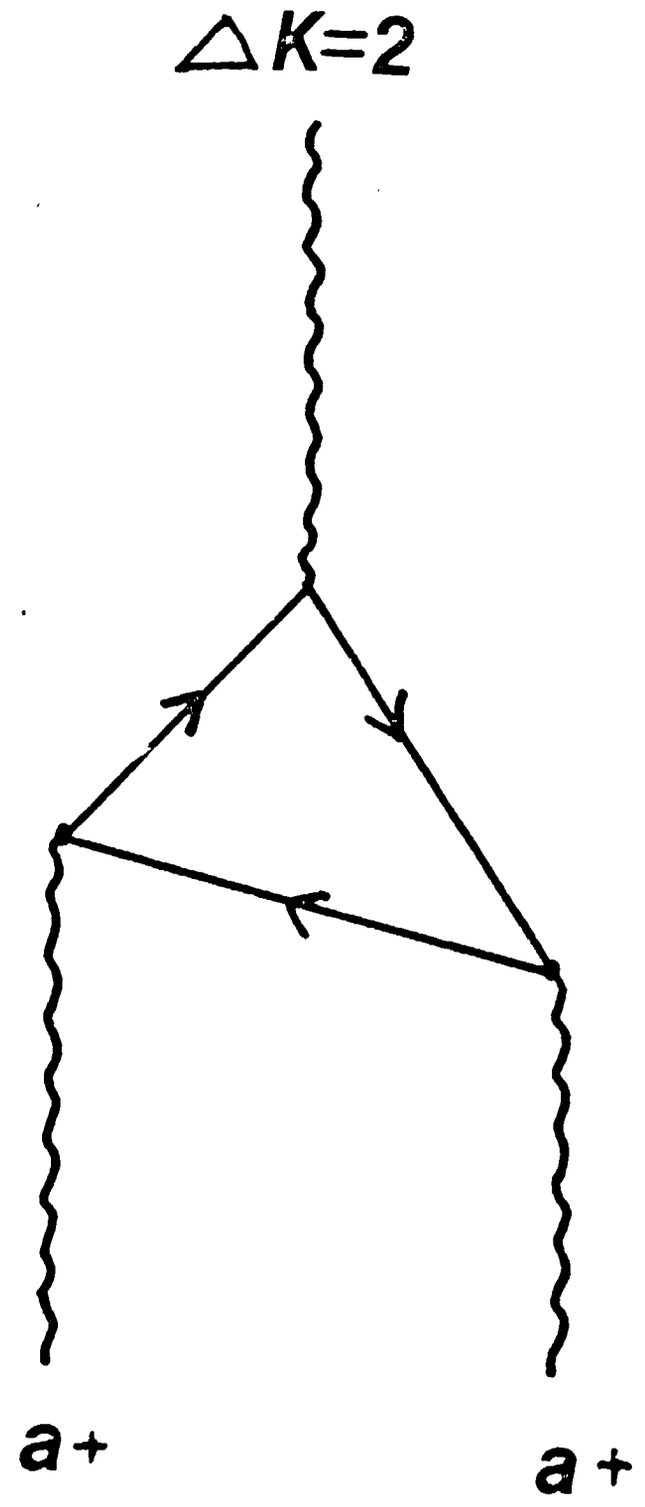

FIG. 7

^{212}Rn

$K^{\pi} = 23^{-}$

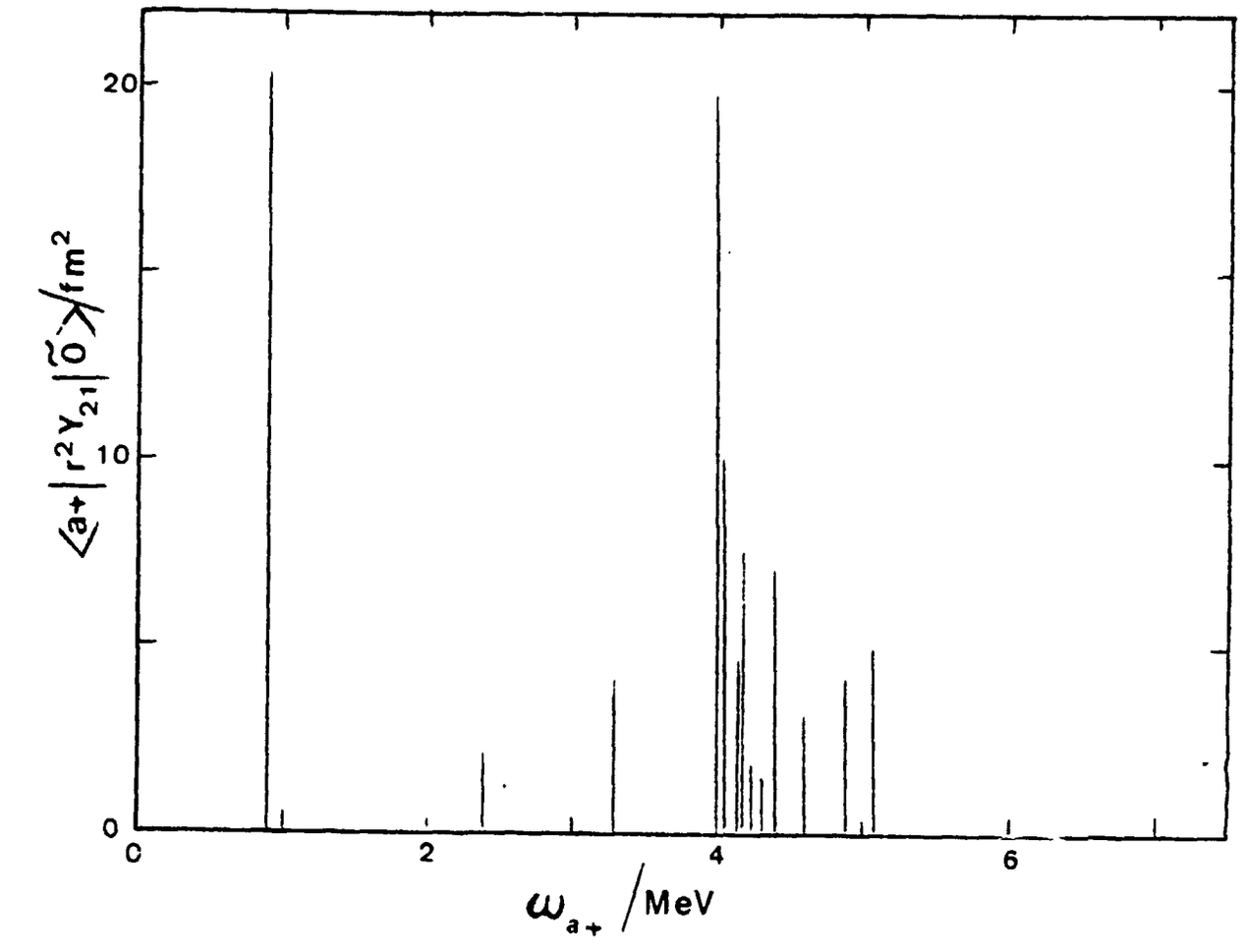

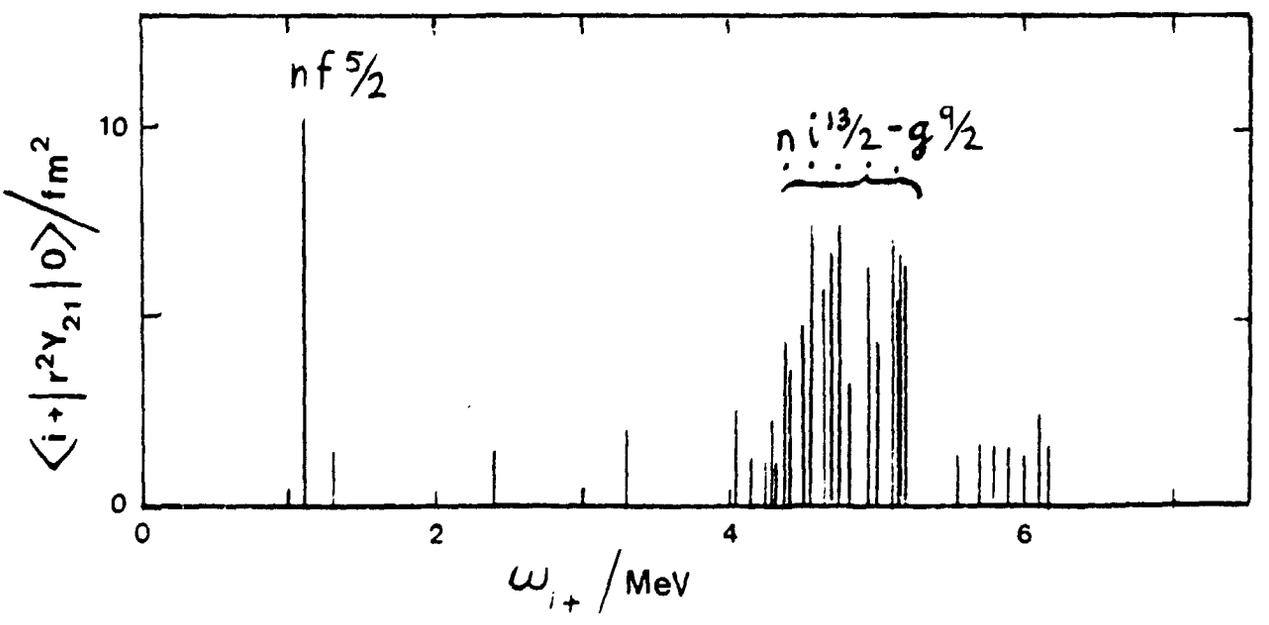

FIG. 3

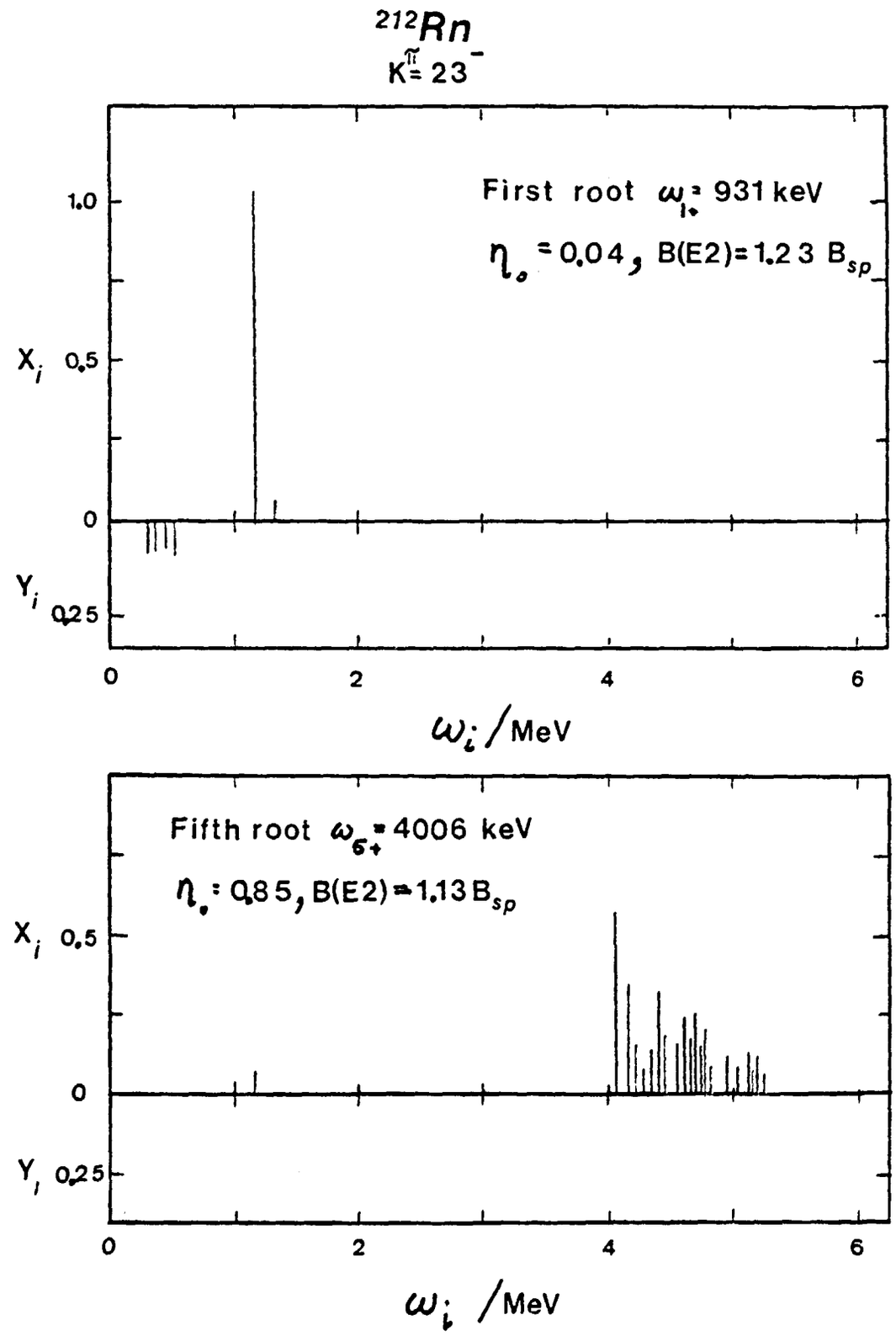
^{212}Rn
$K^{\pi}=23^{-}$
First root ω_{1+} = 931 keV
η_o = 0.04, B(E2) = 1.23 B_{sp}
X_i
Y_i
1.0
0.5
0
0.25
0
2
4
6
ω_i /MeV
Fifth root ω_{6+} = 4006 keV
η_o = 0.85, B(E2) = 1.13 B_{sp}
X_i
Y_i
0.5
0
0.25
0
2
4
6
ω_i /MeV

FIG. 9

^{176}Hf
$K^{\pi}=14^{-}$

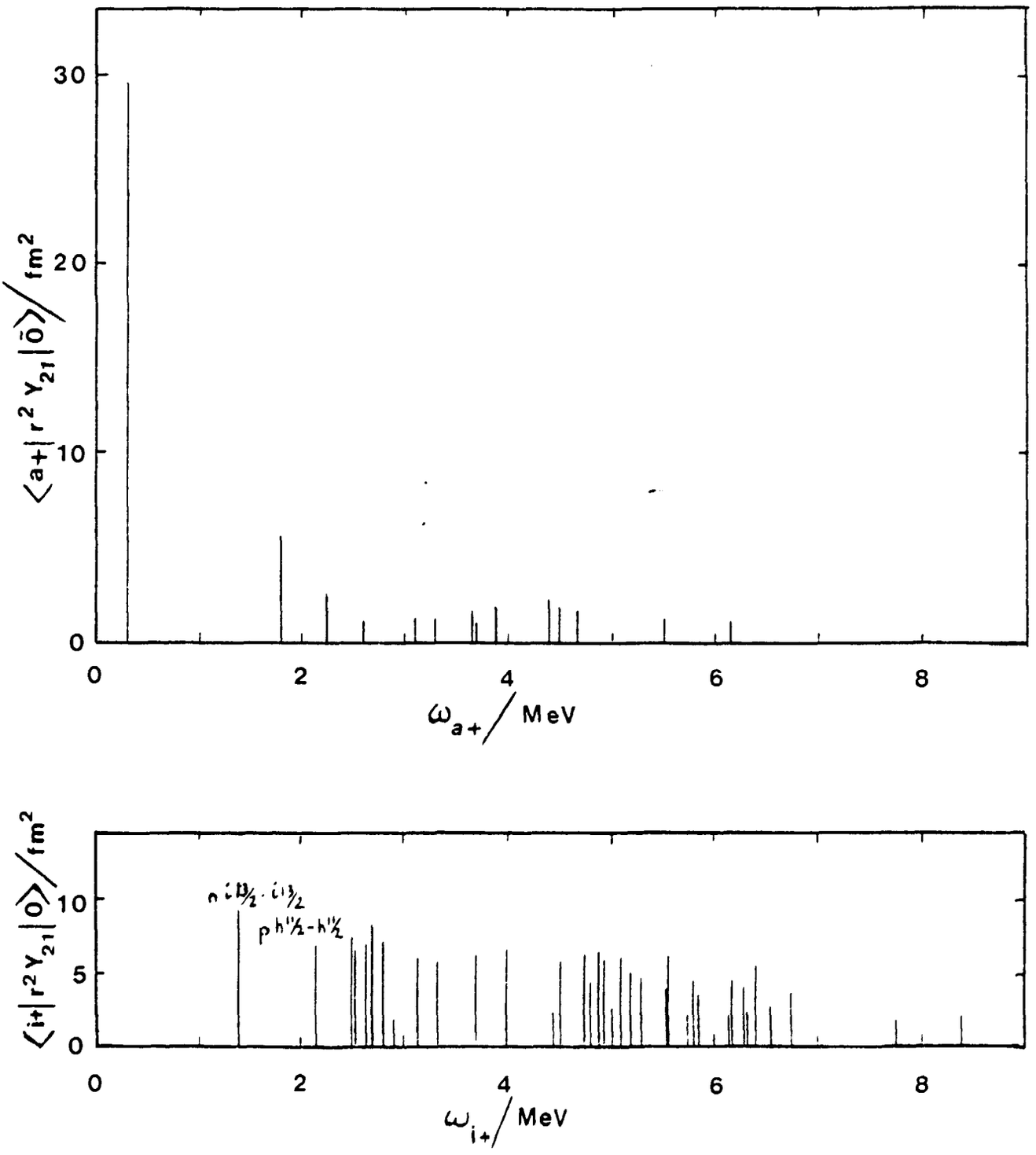

FIG. 10

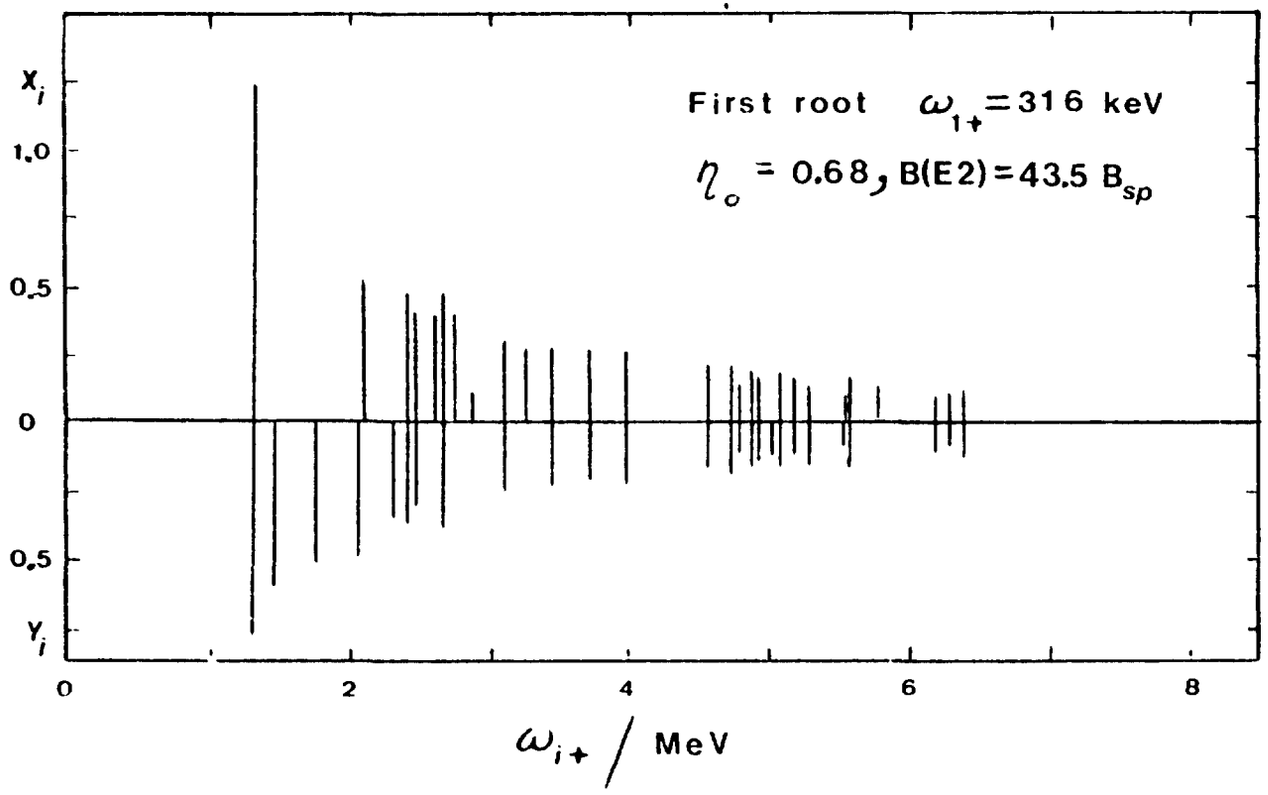

^{176}Hf

$K^{\pi} = 14^-$

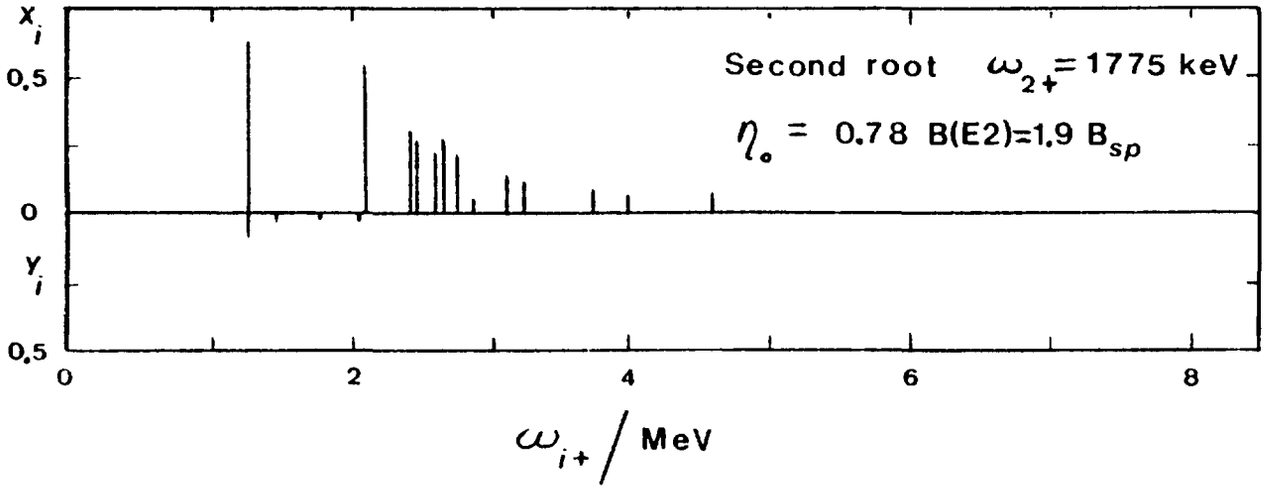

FIG. 11

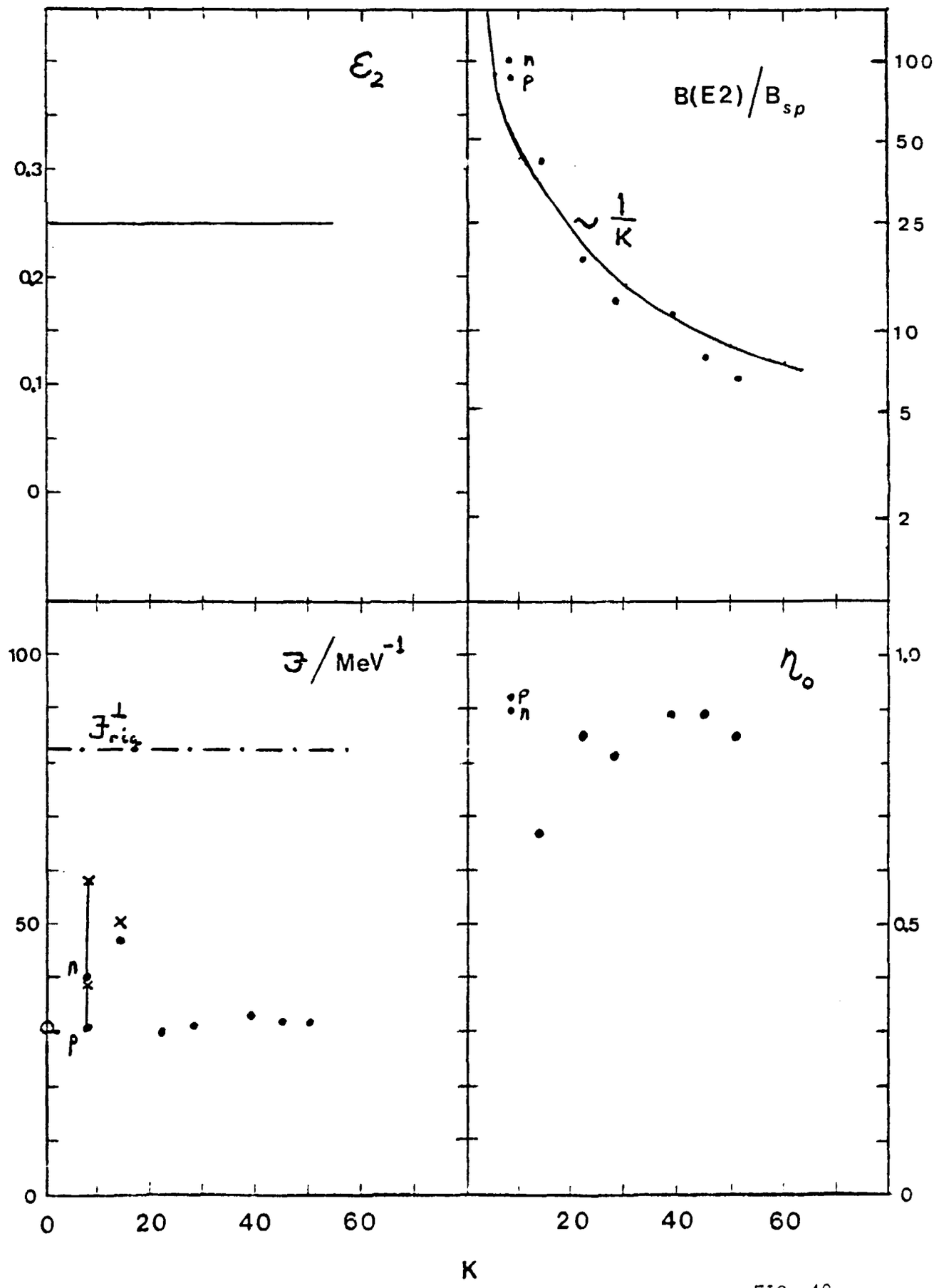
^{176}Hf
ε_2
B(E2)/B$_{sp}$
$\sim \frac{1}{K}$
n
p
$\mathcal{J}$/MeV^{-1}
$\mathcal{J}^{\perp}_{rig}$
η_o
0.3
0.2
0.1
0
100
50
25
10
5
2
1.0
0.5
0
20
40
60
K

FIG. 12

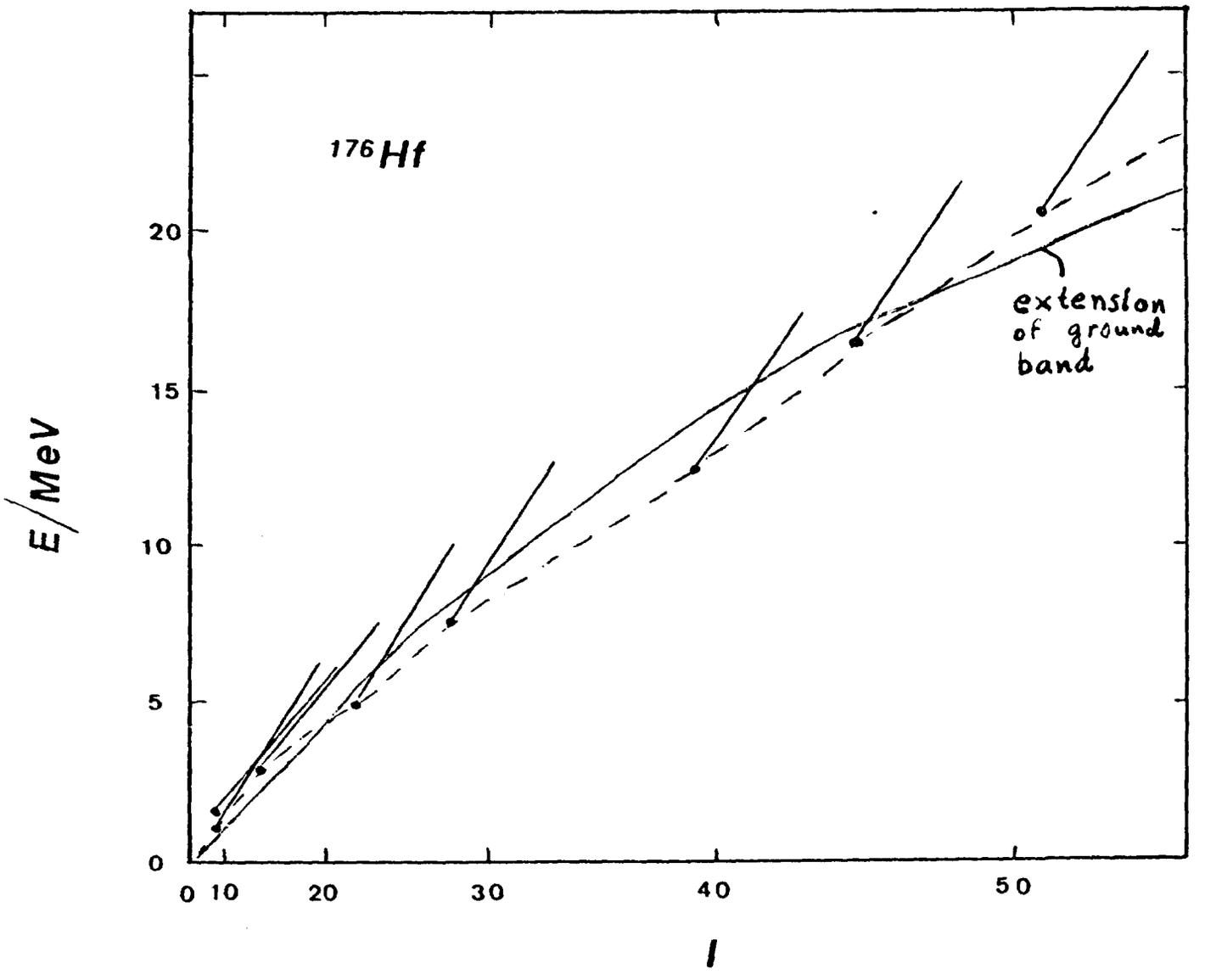
^{176}Hf
E/MeV
I
0
5
10
15
20
0 10
20
30
40
50
extension of ground band

FIG. 13

^{212}Rn

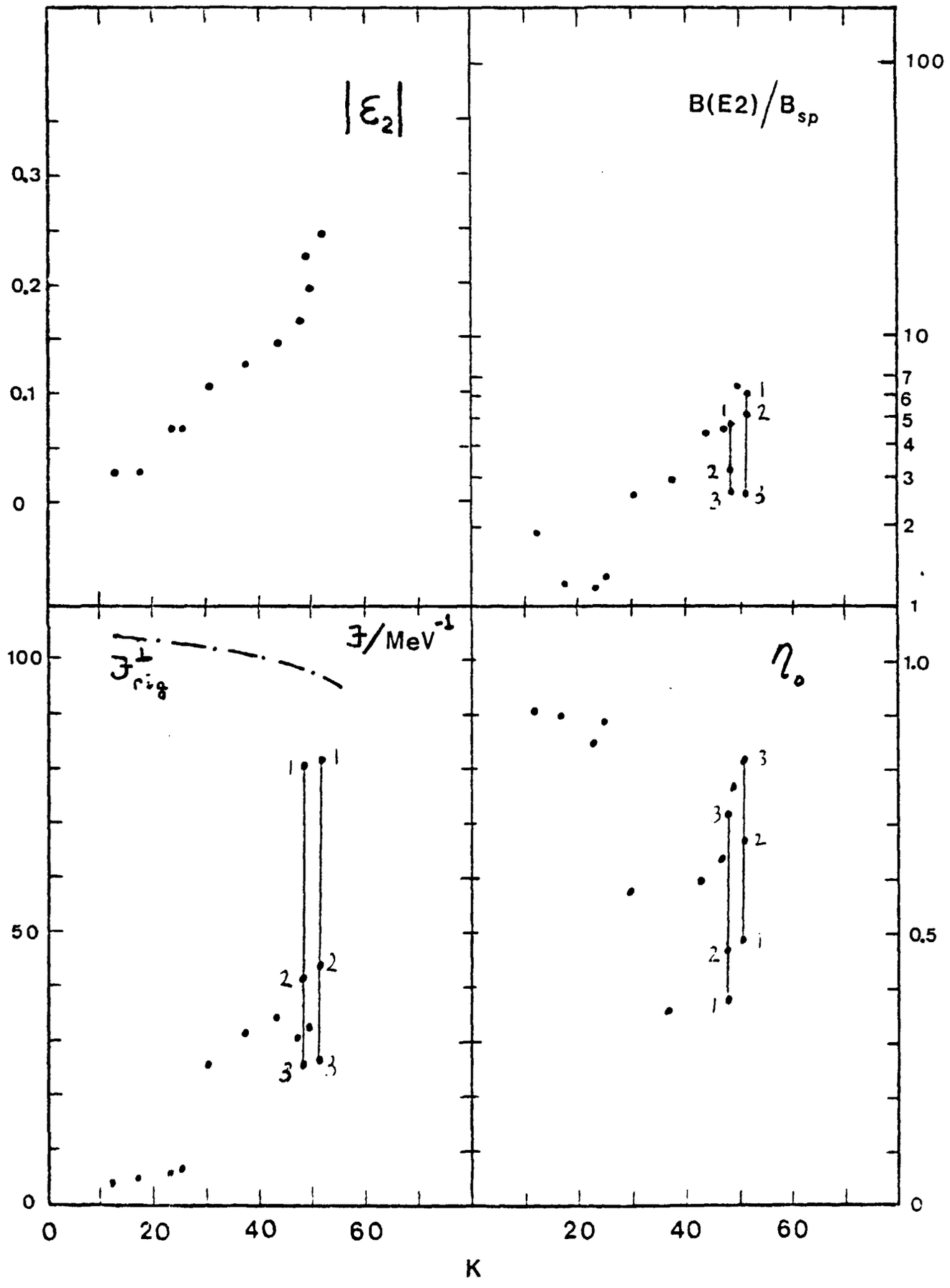
$|\varepsilon_2|$
$B(E2)/B_{sp}$
$\mathcal{I}/MeV^{-1}$
$\mathcal{I}^{-1}_{rig}$
η_o
0.3
0.2
0.1
0
100
10
7
6
5
4
3
2
1
1.0
0.5
50
0
20
40
60
K

FIG. 14

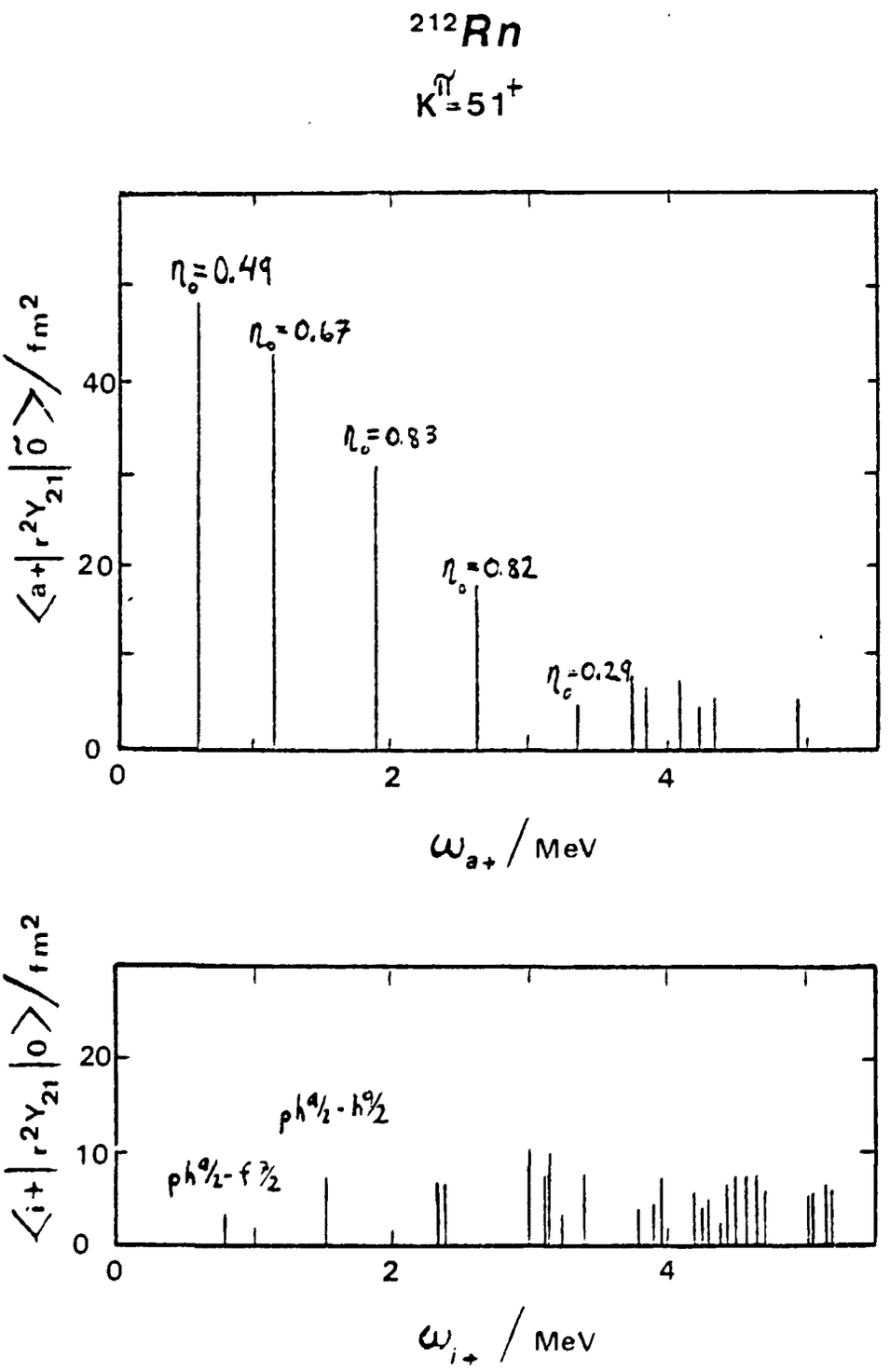
^{212}Rn
$K^{\pi}=51^{+}$
$\eta_o=0.49$
$\eta_o=0.67$
$\eta_o=0.83$
$\eta_o=0.82$
$\eta_o=0.29$
$\langle a+|r^2Y_{21}|0\rangle$ / fm^2
ω_{a+} / MeV
$ph^{9/2}-h^{9/2}$
$ph^{9/2}-f^{7/2}$
$\langle i+|r^2Y_{21}|0\rangle$ / fm^2
ω_{i+} / MeV

FIG. 15

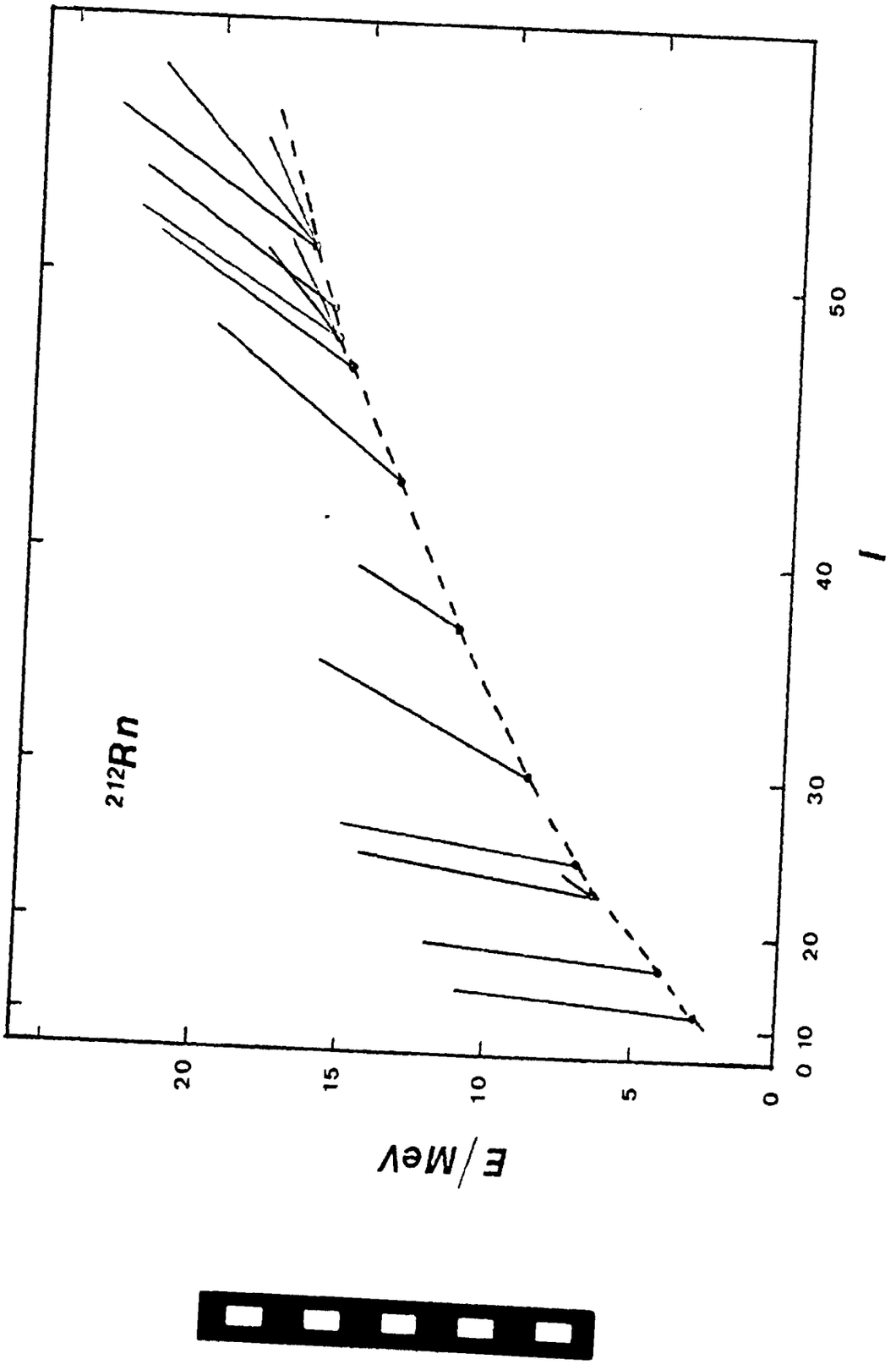

FIG. 16